

# Filling the Gap in Cluster Evolution: JWST's Glimpse into a Young, Star-Forming Cluster at Cosmic Noon

PIERLUIGI RINALDI,<sup>1,2</sup> STACEY ALBERTS,<sup>3,2</sup> CHRISTOPHER N. A. WILLMER,<sup>2</sup> COURTNEY CARREIRA,<sup>4</sup>  
CHRISTINA C. WILLIAMS,<sup>5</sup> GAËL NOIROT,<sup>1</sup> CARYS J. E. GILBERT,<sup>6</sup> ANDREW J. BUNKER,<sup>7</sup> WILLIAM M. BAKER,<sup>8</sup>  
LUIGI BARCHIESI,<sup>6</sup> ZHIYUAN JI,<sup>2</sup> JIANWEI LYU,<sup>2</sup> SANDRO TACCHELLA,<sup>9,10</sup> ZIHAO WU,<sup>11</sup> AND YONGDA ZHU<sup>2</sup>

<sup>1</sup>Space Telescope Science Institute, 3700 San Martin Drive, Baltimore, Maryland 21218, USA

<sup>2</sup>Steward Observatory, University of Arizona, 933 North Cherry Avenue, Tucson, AZ 85721, USA

<sup>3</sup>AURA for the European Space Agency (ESA), Space Telescope Science Institute, 3700 San Martin Dr., Baltimore, MD 21218, USA

<sup>4</sup>Department of Astronomy and Astrophysics, University of California, Santa Cruz, 1156 High Street, Santa Cruz, CA 95064, USA

<sup>5</sup>NSF National Optical-Infrared Astronomy Research Laboratory, 950 North Cherry Avenue, Tucson, AZ 85719, USA

<sup>6</sup>Department of Astronomy, University of Cape Town, Private Bag X3, Rondebosch 7701, South Africa

<sup>7</sup>Department of Physics, University of Oxford, Denys Wilkinson Building, Keble Road, Oxford OX13RH, UK

<sup>8</sup>DARK, Niels Bohr Institute, University of Copenhagen, Jagtvej 128, DK-2200 Copenhagen, Denmark

<sup>9</sup>Kavli Institute for Cosmology, University of Cambridge, Madingley Road, Cambridge, CB3 0HA, UK

<sup>10</sup>Cavendish Laboratory, University of Cambridge, 19 JJ Thomson Avenue, Cambridge, CB3 0HE, UK

<sup>11</sup>Center for Astrophysics | Harvard & Smithsonian, 60 Garden St., Cambridge MA 02138 USA

Submitted to ApJ

## ABSTRACT

We present a detailed study of HUDFJ0332.4–2746.6 (HUDF46), a  $z \approx 1.84$  overdensity in the Hubble Ultra Deep Field, previously identified with HST as a proto-cluster. JWST/NIRISS spectroscopy expands its confirmed membership from 18 to 37 galaxies, while deep HST/ACS, JWST/NIRCam, and JWST/MIRI imaging provide a comprehensive multiwavelength view from the rest-frame UV to the mid-infrared. This dataset probes the population across three dex in stellar mass ( $M_{\star} \approx 10^{7.5-10.5} M_{\odot}$ ), delivering the first direct view of a young cluster down to such low- $M_{\star}$  at  $z \gtrsim 1$ . Assuming virialization, we derive a velocity dispersion of  $\sigma \approx 670 \pm 91 \text{ km s}^{-1}$  and a halo mass of  $M_{200} \approx (1.2 \pm 0.2) \times 10^{14} M_{\odot}$ , in agreement with X-ray constraints from deep *Chandra* data. Despite residing in a massive halo likely in the hot-halo regime, the population is overwhelmingly star-forming, with no established red sequence and no extended X-ray emission from a hot intracluster medium. HUDF46 members have stellar and structural properties nearly indistinguishable from coeval field galaxies, and the structure hosts only one AGN candidate, found in its brightest galaxy, which lies at the cluster center. Overall, HUDF46 appears to be in a transitional phase prior to the onset of environmental quenching, making its galaxy population a key benchmark for tracing the processes that will later build a passive population and shape the assembly of massive clusters at later cosmic times.

**Keywords:** Galaxy evolution (594); Galaxy formation (595); Spectral energy distribution (2129); High-redshift galaxies (734); Dwarf galaxies (416); Galaxy environments (2029); Galaxy quenching (2040)

## 1. INTRODUCTION

In the  $\Lambda$ CDM cosmological framework, structure formation proceeds through the collapse of primordial

density fluctuations into dark matter halos (Press & Schechter 1974; White & Rees 1978). Baryons subsequently fall into these potential wells, cool, and form stars, giving rise to galaxies. As gravity drives the hierarchical growth of structure, halos merge into increasingly massive systems, eventually forming the largest gravitationally bound structures in the Universe: galaxy

clusters, which host hundreds to thousands of galaxies (Kravtsov & Borgani 2012).

Given their cosmological importance, galaxy clusters have long been the focus of extensive observational and theoretical studies, revealing a strong connection between galaxy properties and environment. Early evidence for this link was provided by Butcher & Oemler (1978) and later on by Dressler (1980), who showed that galaxies in dense regions exhibit distinct morphologies and colors compared to field galaxies at low redshift. Subsequent work has confirmed and extended these results across cosmic time (see Dressler 1984; Boselli & Gavazzi 2006; De Lucia et al. 2007; Blanton & Moustakas 2009; Boselli et al. 2014; Alberts & Noble 2022, and references therein), demonstrating that environmental processes play a fundamental role in driving galaxy evolution (e.g., Peng et al. 2010; Thomas et al. 2010).

As observations extended to higher redshift, studies showed that environmental effects are already in place at  $z \gtrsim 1$  (e.g., Rettura et al. 2011; Muzzin et al. 2012; Noble et al. 2013; Balogh et al. 2016; Kawinwanichakij et al. 2017; Ji et al. 2018), with field galaxies assembling their stellar mass ( $M_{\star}$ ) over longer timescales, while cluster galaxies are predominantly early-type galaxies (ETGs), defining what is now commonly defined as a red sequence in galaxy clusters, with smooth, ellipsoidal structures and old stellar populations out to  $z \approx 1.5$ – $2$  (see Alberts & Noble 2022). Together, these results indicate that dense environments accelerate galaxy evolution and quenching (e.g., Mei et al. 2009; Stanford et al. 2012; Muzzin et al. 2013), with such signatures already in place at high redshift (e.g., Li et al. 2025), motivating constraints on their underlying mechanisms and onset epoch.

However, *how do these processes take place?* In massive dark matter halos tracing group- and cluster-scale structures, gas is expected to be shock-heated to high virial temperatures, suppressing cold accretion and establishing a hot intracluster medium (ICM; Birnboim & Dekel 2003; Dekel & Birnboim 2006). The presence of a hot ICM is typically adopted as a signpost of already virialized, massive systems (Foley et al. 2011; Mantz et al. 2020), through its detection in X-ray emission (Sarazin 1986) and via the Sunyaev–Zel’dovich effect (Birkinshaw 1999)<sup>1</sup>. Galaxies accreting onto these halos may experience ram-pressure stripping and tidal perturbations (Gunn & Gott 1972; Moore et al. 1998), potentially even before full cluster infall (Berrier et al.

2009; McGee et al. 2009). In parallel, increasingly efficient feedback from Active Galactic Nuclei (AGNs), both energetic and maintenance modes, can further regulate gas cooling and re-accretion (Croton et al. 2006; Henriques et al. 2017). Although halo assembly is well characterized, the epoch at which these environmental processes begin to significantly affect galaxies remains empirically uncertain.

Addressing *when* and *how* these transformations occur requires observing clusters during their early assembly phase, before environmental processes have fully reshaped their galaxy populations. At this stage, these systems lack a developed hot ICM, rendering them undetectable through classical methods (e.g., X-ray and Sunyaev–Zel’dovich). At these early stages, structures commonly identified as protoclusters or overdensities are not yet virialized, and at high redshift not all overdensities are expected to collapse into present-day clusters (Muldrew et al. 2015). As a result, the distinction between groups, clusters, and protoclusters is often applied pragmatically, since observational limitations rarely permit an unambiguous classification (see Overzier 2016).

With the advent of JWST (Gardner et al. 2023), the identification and characterization of galaxy overdensities and group-scale structures—likely progenitors of present-day clusters—has become increasingly routine, owing to the unprecedented depth and resolution of NIRCcam (Rieke et al. 2023) and MIRI (Wright et al. 2023). These capabilities enable the detection of overdense regions even during the Epoch of Reionization (Helton et al. 2024; Fudamoto et al. 2025; Wu et al. 2026). Crucially, JWST now allows us to probe the low-mass regime within these structures, revealing that low-mass quiescent galaxies may follow evolutionary pathways distinct from their massive counterparts. Recent analyses (see discussion in Cutler et al. 2025) suggest that, at  $z \gtrsim 2$ , the initial quenching of low-mass systems is not predominantly environmentally driven, and may instead reflect bursty or temporarily suppressed star formation (e.g. Tacchella et al. 2016), with long-timescale environmental mechanisms becoming dominant only at later epochs. Access to the low-mass population is therefore essential to disentangle the onset of quenching from the subsequent environmental processing that ultimately reshapes galaxies in dense environments.

Therefore, identifying cluster- and protocluster-scale overdensities represents only the first step toward understanding the formation of massive cosmic structures observed at later epochs. A complete picture requires determining their evolutionary stage and fully characterizing their galaxy populations by (1) establishing robust membership across a wide mass range, from the

<sup>1</sup> Searches for clusters using these methods have historically been biased toward more mature, already virialized systems.

most massive systems to the faintest low-mass galaxies, and (2) constraining their stellar populations and star-formation histories. Only by linking galaxy demographics to their physical properties can we reconstruct the pathway from assembling protoclusters to mature clusters, and quantify how environmental processes shape galaxy evolution across cosmic time.

In this paper, we study HUDFJ0332.4–2746.6 (hereafter HUDF46), an overdensity at  $z = 1.84 \pm 0.01$  in the Hubble Ultra Deep Field (HUDF; Beckwith et al. 2006), identified by Mei et al. (2015) as a protocluster with an estimated halo mass of  $M_{200} = (2.2 \pm 1.8) \times 10^{14} M_{\odot}$ , an intrinsic velocity dispersion ( $\sigma$ ) of  $730 \pm 260 \text{ km s}^{-1}$  and  $R_{200} = 0.9 \pm 0.3 \text{ Mpc}^2$ . The halo mass was inferred assuming virialization, based on the Gaussian velocity distribution of member galaxies, the detection of an  $18\sigma$  overdensity consistent with a massive node of the cosmic web (Hahn et al. 2007; Cautun et al. 2014), and upper limits from 4 Ms *Chandra* X-ray observations (Xue et al. 2011). Mei et al. (2015) showed that HUDF46 lacks a well-defined red sequence (i.e., missing quenched galaxies) and suggested the presence of a substantial population of star-forming ETGs in a dense environment at these redshifts. Here, we exploit new ultra-deep JWST observations obtained with NIRCcam, MIRI, and, critically, the Near Infrared Imager and Slitless Spectrograph (NIRISS; Willott et al. 2022; Doyon et al. 2023), which provide robust spectroscopic redshifts. This leap in sensitivity allows us to revisit and significantly extend the analysis of Mei et al. (2015) by probing its member galaxies across three dex in stellar mass ( $M_{\star} \approx 10^{7.5-10.5} M_{\odot}$ ). By revising its membership and incorporating low-mass members, HUDF46 provides a uniquely powerful laboratory for studying cluster evolution in action, enabling a direct assessment of how environmental mechanisms begin to shape galaxy populations across a wide range in stellar mass.

This paper is structured as follows. Section 2 presents the dataset used in this work. Section 3 outlines the sample selection and redshift assessment. Section 4 details the methodology adopted to identify HUDF46. Section 5 presents a detailed analysis of HUDF46 and its galaxy population in comparison to coeval field galaxies. Section 6 summarizes and discusses the main results. Throughout this paper, we consider a cosmology with  $H_0 = 70 \text{ km s}^{-1} \text{ Mpc}^{-1}$ ,  $\Omega_M = 0.3$ , and  $\Omega_{\Lambda} = 0.7$ . All magnitudes are total and refer to the AB system (Oke

<sup>2</sup>  $R_{200}$  is the radius within which the mean cluster density equals 200 times the critical density of the Universe.

& Gunn 1983). A Kroupa (2001) initial mass function (IMF) is assumed ( $0.1-100 M_{\odot}$ ).

## 2. DATASET

We relied on HST and JWST data available in HUDF. This section describes all datasets used, with particular focus on the reduction of NIRISS data (imaging and wide field slitless spectroscopy). We emphasize that in NIRISS wide-field slitless spectroscopy observations, the associated NIRISS direct imaging serves as pre-imaging to support the grism data reduction, providing source positions, extraction apertures, and contamination estimates. In contrast, the photometry in the NIRISS wavelength range (F115W, F150W, F200W) used for spectral energy distribution (SED) fitting is derived from the corresponding NIRCcam imaging, which is significantly deeper. This approach ensures a more robust photometric characterization of faint galaxies, while all spectroscopic measurements are obtained exclusively from the NIRISS grism observations.

### 2.1. HST

As for the HST data, we used the ACS/WFC and WFC3/IR data from the Hubble Legacy Field (HLF) observations that cover GOODS-S. The HLF provides deep imaging in 9 HST bands covering a wide range of wavelengths ( $0.4-1.6 \mu\text{m}$ ), from the optical (ACS/WFC F435W, F606W, F775W, F814W, and F850LP filters) to the near-infrared (WFC3/IR F105W, F125W, F140W and F160W filters). In this work, we make use of HST/ACS only for our analysis, since the overlap of HST/WFC3 with NIRCcam. For a more detailed description of this dataset, we refer the reader to Whitaker et al. (2019).

### 2.2. NIRCcam

We made use of NIRCcam data from the JWST Advanced Deep Extragalactic Survey (JADES) NIRCcam Data Release 2 (JADES DR2 – PIDs: 1180, 1210; PIs.: D. Eisenstein, N. Luetzgendorf; Eisenstein et al. 2023a,b), which includes observations from the JWST Extragalactic Medium-band Survey (JEMS – PID: 1963; PIs.: C. C. Williams, S. Tacchella, M. Maseda; Williams et al. 2023) and the First Reionization Epoch Spectroscopically Complete Observations (FRESCO – PID: 1895; PI: P. Oesch; Oesch et al. 2023).

The combined NIRCcam data from all these surveys data cover a broad wavelength range ( $\approx 1-5 \mu\text{m}$ ): F090W, F115W, F150W, F182M, F200W, F210M, F277W, F335M, F356W, F430M, F444W, F460M, and F480M. For more details, we refer the reader to the JADES DR2 (Eisenstein et al. 2023a,b).

### 2.3. MIRI

We also considered MIRI data from the SMILES program (PID: 1207; PI: G. H. Rieke, Rieke et al. 2024), which enable us to cover a wide range of wavelengths, from  $5.6 \mu\text{m}$  to  $25.5 \mu\text{m}$ . A more detailed discussion on the MIRI data reduction and overall quality of the data can be found in Alberts et al. (2024) for SMILES.

### 2.4. NIRISS

We made use of imaging and wide-field slitless spectroscopy (WFSS) data from the Next Generation Deep Extragalactic Exploratory Public (NGDEEP) program (PID 2079, PIs: S. Finkelstein, C. Papovich, N. Pirzkal), which covers HUDF with three filters (F115W, F150W, and F200W) over  $\approx 5.4 \text{ arcmin}^2$  with a 1D line sensitivity ( $5\sigma$ ) of  $\approx 1.3 \times 10^{-18} \text{ erg s}^{-1} \text{ cm}^{-2}$ . We refer the reader to Shen et al. (2024), Forrey et al. (2025), and Shen et al. (2025) for more details on the NGDEEP dataset.

The data were reduced with our custom NIRISS pipeline, which incorporates additional steps originally developed for NIRCcam and MIRI image processing and already applied in several recent works (e.g., Rinaldi et al. 2023; Caputi et al. 2024; Iani et al. 2024; Navarro-Carrera et al. 2024b; Rinaldi et al. 2025). The NIRISS pipeline is built on the official JWST pipeline (1.16.1; pmmap\_1303) and the GRIZLI pipeline (1.12.8; Brammer & Matharu 2021). We refer the reader to the Appendix A, which provides a schematic overview of the full reduction workflow.

## 3. SAMPLE SELECTION AND REDSHIFT EVALUATION

Since our goal is to better characterize HUDF46, reported by Mei et al. (2015), we restricted our analysis to galaxies within the redshift range  $z_{\text{phot}} \approx 1.5 - 2.5$ . Accordingly, we pre-selected sources directly from the JADES DR2 catalog based on their photometric redshifts (Hainline et al. 2024).

We then made use of GRIZLI to extract all pre-selected sources from the JADES DR2 catalog blindly (i.e., without applying any prior from the photometric redshifts during the fit with GRIZLI). The main advantage of using GRIZLI is its ability to forward-model templates directly onto the 2D grism frames, incorporating source morphology to account for spectral smearing across adjacent pixels in the direct image. Most importantly, GRIZLI allows us to also model and remove, during the fitting process, nearby sources that can potentially contaminate the source of interest. We fit the grism data using GRIZLI, simultaneously incorporating information from both orthogonal grisms. In this context, for the

fitting process and redshift estimation, GRIZLI employs templates based on flexible stellar population synthesis models (Conroy & Gunn 2010), combined with nebular emission lines.

When GRIZLI extracts and fits each object, it generates multiple output files (\*.fits and \*.png), allowing users to inspect both 1D and 2D spectra (for each grism-filter combination) alongside the extracted spectra and their redshift probability distribution functions (PDFs). If GRIZLI fails to fit the extracted spectrum, it still produces all the aforementioned files except for the fitted spectrum and its corresponding probability distribution function (PDF).

Once GRIZLI completed the extraction, we performed multiple tiers of visual inspection. The first tier classified sources into four categories based on their redshift reliability:

- **FLAG 1:** Sources with a secure redshift solution based on both the 1D and 2D spectra, supported by the detection of multiple emission lines and characterized by either a single peak or a dominant peak ( $\gtrsim 90\%$  of the PDF).
- **FLAG 2:** Sources where the redshift solution was less certain, resulting in multiple peaks in the PDF without a single dominant solution, either due to faintness or single-line detections, with the quality of the identification assessed using  $z_{\text{phot}}$  in the second round of inspection.
- **FLAG 3:** Sources for which neither the 1D nor 2D spectra yielded a reliable redshift solution, typically due to a chaotic PDF, severe contamination from instrumental artifacts (e.g., lightsaber effects or unflagged snowballs<sup>3</sup>), or their location at the edge of the grism exposures, resulting in poor spectral coverage.
- **FLAG 4:** Sources for which GRIZLI failed to converge to any reliable redshift solution<sup>4</sup>.

In the second tier, we reviewed only FLAG 1 and FLAG 2 sources to minimize potential outliers from GRIZLI. Some were downgraded to FLAG 3 and discarded due to unreliable redshift solutions (e.g., strong 2D contamination), while a subset of FLAG 2 sources were upgraded to FLAG 1 when single-line identifications were

<sup>3</sup> See NIRISS Known Issues (JDox) and NIRCcam Known Issues (JDox)

<sup>4</sup> Some of these objects exhibit clear emission lines but a poorly constrained or unreliable continuum, preventing a robust joint fit of continuum and line emission from GRIZLI.

supported by the photometric redshifts enabled by the dense HST+NIRCam coverage in HUDF. The third tier focused on FLAG 4 sources. Since GRIZLI does not provide any redshift for this class by default during the extraction process due to poorly constrained or unreliable continuum, we forced the fits using JADES DR2 photometric redshifts as priors, assuming a 10% uncertainty and adopting a fine redshift grid ( $dz = 0.0004$ ) centered on the prior value (following Watson et al. 2025b). This process allowed us to recover several sources (e.g., with clear emission lines), which were then reclassified as either FLAG 1 or FLAG 2 based on their PDFs, while others were reassigned to FLAG 3 and discarded. When possible, we also made use of spectroscopic redshifts available in the field from 3D-HST (Brammer et al. 2012), MUSE Hubble Ultra-Deep Field (Bacon et al. 2023), FRESCO (Oesch et al. 2023), ASPECS (Walter et al. 2016), and recent Near-Infrared Spectrograph (NIRSpec; Ferruit et al. 2022; Jakobsen et al. 2022) observations from JADES (D’Eugenio et al. 2024) and SMILES (Zhu et al. 2025). At this point, our sample includes only three quality flags: 1, 2, and 3.

Finally, we reviewed all sources classified as FLAG 1 and FLAG 2, leveraging all available information to refine our final assessment, thus including spectral energy distributions (SEDs) from JADES and postage stamps across HST and JWST filters.

At the end of this multi-tiered inspection, we obtain 259 sources with FLAG 1, 54 with FLAG 2, and 303 with FLAG 3. We notice that most FLAG 3 sources are either low-mass galaxies (with 85% having  $\lesssim 10^8 M_\odot$ ) or lie in regions of the NIRISS/WFSS footprint where information cannot be reliably extracted due to edge effects or severe contamination from nearby sources (see Figure 1).

In Figure 2, we show the comparison between our FLAG 1 (i.e., the sources we will focus on throughout this work) with the available spectroscopic redshifts in HUDF from 3D-HST, MUSE Hubble Ultra-Deep Field, FRESCO, ASPECS, and recent NIRSpec observations from JADES and SMILES. We find a relatively small outlier fraction of 4.8% (where outliers are defined as  $|\Delta z| > 0.15$ ;  $N_{\text{matched}} = 125$ ). The normalized median absolute deviation is  $\sigma_{\text{NMAD}} = 0.004$ , indicating tight agreement between  $z_{\text{NIRISS}}$  and  $z_{\text{spec}}$ , while the standard deviation of  $\sigma_{\text{std}} = 0.084$  reflects a small tail of larger deviations (see black box). As shown in Figure 2, some sources (highlighted with red squares; specifically, sources: 3, 4, 5, and 6) were classified at much higher redshifts than what we infer from NIRISS/WFSS. We visually inspected these outliers (see RGB postage stamps from NIRCam F090W, F115W, and F150W),

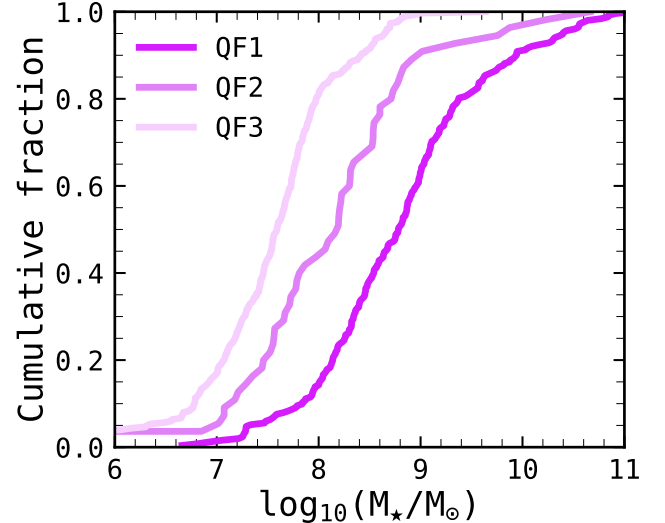


**Figure 1.** Stellar mass distributions of galaxies grouped by quality flag of their redshift (QF1, QF2, QF3), shown as cumulative fractions to enable direct comparison between the samples. For QF1 sources, stellar masses are derived in this work by fixing the redshift to the spectroscopic value (see Section 5.4.1), while for QF2 and QF3 sources stellar masses are taken from existing field catalogs and are based on photometric redshifts (Rinaldi et al. 2024; Navarro-Carrera et al. 2024a). The vast majority of galaxies in QF3 ( $\approx 80\text{--}85\%$ ) have stellar masses below  $\approx 10^8 M_\odot$ .

and find that their photometric redshifts agree well with our NIRISS-based spectroscopic redshifts. Further inspection of their SEDs confirms that these sources are not at high redshift (as initially pointed out in the previous literature), and we conclude that their published  $z_{\text{spec}}$  values are likely the result of unreliable quality flags (either from MUSE or 3D-HST). After removing these sources, the agreement between  $z_{\text{NIRISS}}$  and  $z_{\text{spec}}$  improves further, reducing the outlier fraction to 1.7% (see red box).

We also assessed the agreement between our  $z_{\text{NIRISS}}$  estimates and the photometric redshifts from JADES DR2, finding an outlier fraction of 3.4%, with  $\sigma_{\text{NMAD}} = 0.031$  and  $\sigma_{\text{std}} = 0.161$ , indicating overall good consistency despite a broader tail.

#### 4. IDENTIFICATION OF OVERDENSITIES IN HUDF

Identifying galaxy overdensities is non-trivial. Spectroscopic samples provide robust redshifts but suffer from sparse sampling and complex selection functions, limiting classical density–contrast methods that assume uniform coverage. Slitless spectroscopy (e.g., NIRISS) offers more homogeneous sampling and is less sensitive to edge effects and bright neighbors than imaging, though incompleteness persists due to 1) spectral

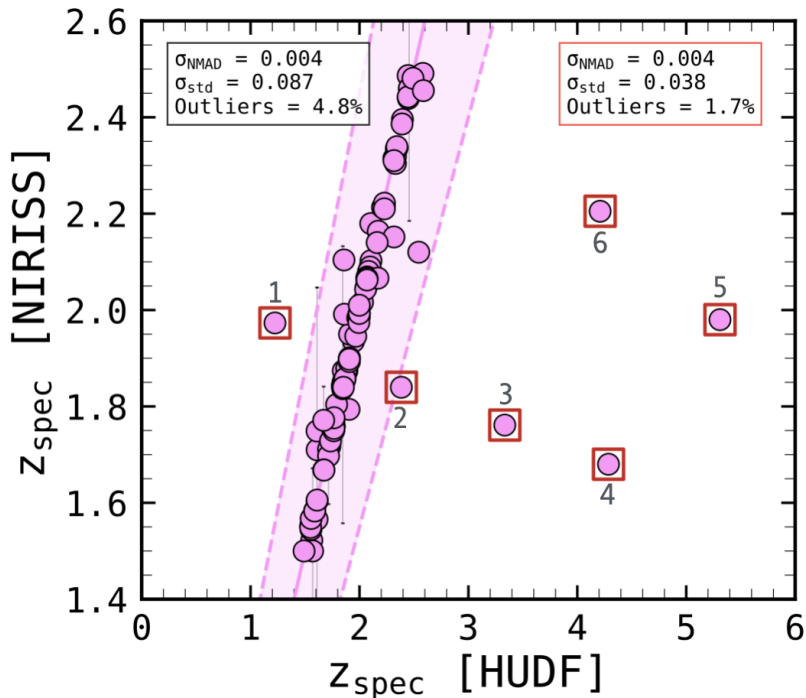


**Figure 2.** We perform a benchmark comparison between our spectroscopic redshifts from NIRISS/WFSS and those available in the HUDF from 3D-HST, MUSE, FRESCO, ASPECS, and recent NIRSpc observations from JADES and SMILES (only their QF=1). The left panel shows the comparison between the redshifts measured here with previous results. Overall, we find good agreement with the existing literature (black box, top left). The right panel highlights the few outliers (denoted by numbers on the left panel) which we visually inspected. We find that the sources previously spectroscopically classified as high-redshift objects are likely affected by unreliable quality flags in the earlier datasets. Their photometric redshifts (from JADES DR2) agree well with our NIRISS-based spectroscopic redshifts, further supporting the revised lower-redshift interpretation. After removing these sources, the agreement between  $z_{\text{NIRISS}}$  and  $z_{\text{HUDF}}$  improves further (red box, top right).

overlap and 2) ambiguities when only a single line is detected. By contrast, photometric redshifts enable larger, more complete samples but introduce projection effects from their higher uncertainties. To address these challenges, several approaches have been developed, including Voronoi tessellations (e.g., Ramella et al. 2001), adaptive kernel smoothing (e.g., Darvish et al. 2015), and the Friends-of-Friends (FoF) algorithm (e.g., Huchra & Geller 1982; Berlind et al. 2006), with the latter being adopted in this work (see next section).

#### 4.1. Group Identification via Friends-of-Friends and Evidence Accumulation Clustering

In this work, we apply a FoF algorithm to the spectroscopic catalog (Section 3) using a multi-tiered grid of projected separations and velocity differences, thereby avoiding reliance on a single linking choice and capturing a range of plausible groupings. The goal of this section is to identify overdensities within the NIRISS field over the redshift range  $z \approx 1.5$ – $2.5$ , which includes indepen-

dent confirmation of HUDF46 and its properties using the near-IR coverage and sensitivity of NIRISS. FoF is a well-tested group finder in both simulations and redshift surveys, linking galaxies in redshift space based on projected and line-of-sight separations and associating those likely residing within a common dark-matter halo. When properly parameterized, FoF minimizes fragmentation and over-merging, recovers unbiased group multiplicity functions, and yields nearly universal halo mass functions accurate to  $\approx 10\%$  across redshift and cosmology (e.g., Courtin et al. 2011). To assess the robustness of the resulting group catalogs across the FoF parameter space, we also employ a custom framework based on Evidence Accumulation Clustering (EAC; Fred & Jain 2005). The most secure overdensities identified in this way are then used as a benchmark for applying the method of Watson et al. (2025a), which builds upon established observational techniques, including the modified Eisenhardt et al. (2008) criteria introduced by Noirot et al. (2018).

We explored a  $9 \times 20$  grid in the FoF linking parameters. The projected linking length spanned  $r_{\perp} = 0.10$ – $0.50$  Mpc in  $0.05$  Mpc steps, and the line-of-sight velocity threshold  $\sigma = 100$ – $2000$  km s $^{-1}$  in  $100$  km s $^{-1}$  steps. These values were chosen to reflect the NIRISS field of view at  $z \approx 2$  and the typical velocity uncertainty of our spectroscopic redshifts. Each of the resulting FoF runs produced an independent partition  $P^{(r)}$  of galaxies into groups, effectively sampling the possible ways galaxies can be physically connected under different linking assumptions.

Then, the EAC method aggregates these multiple realizations into a single, consensus grouping by interpreting each FoF run as a piece of evidence on the physical association between galaxies. For each galaxy pair  $(i, j)$ , we recorded whether it appeared in the same FoF group across the ensemble of runs, defining the *co-association matrix* as:

$$C_{ij} = \frac{1}{N} \sum_{r=1}^N \mathbf{1}[i, j \in \text{same group in } P^{(r)}], \quad (1)$$

whose entries represent the empirical probability that galaxies  $i$  and  $j$  belong to the same structure. In this framework, FoF provides the base clusterings, while EAC serves as a consensus layer that extracts only those associations that are consistently recovered across the entire parameter grid.

We interpret  $C$  as a similarity matrix and construct an undirected graph using `networkx`, where galaxies are vertices and edges connect pairs with  $C_{ij} \geq \pi_{\min}$ <sup>5</sup>. Varying  $\pi_{\min}$  from  $0.20$  to  $1.00$  in steps of  $0.05$  yields 17 provisional partitions. An edge is considered *robust* if it appears in at least half of these partitions (i.e. in  $\geq 50\%$  of  $\pi_{\min}$  sweeps). The connected components of the resulting *consensus graph* represent the final EAC-refined FoF groups. This ensures that only galaxy associations that persist across both the FoF parameter grid and the EAC threshold space are retained.

For each galaxy  $i$ , we further quantified the stability of its membership through three metrics:

- *Intra-group coherence*,  $P_{\text{group}}(i)$ , the biweight location of  $C_{ij}$  values linking  $i$  to the other members of its consensus group.
- *Grouping frequency*,  $f_{\text{grouped}}(i) = n_i^{\text{grp}}/N_{\text{runs}}$ , the fraction of FoF realizations in which  $i$  appears in *any* group, measuring its overall tendency to cluster.

<sup>5</sup> Where,  $\pi_{\min}$  is the minimum required co-association probability for declaring a link between two galaxies in the EAC graph.

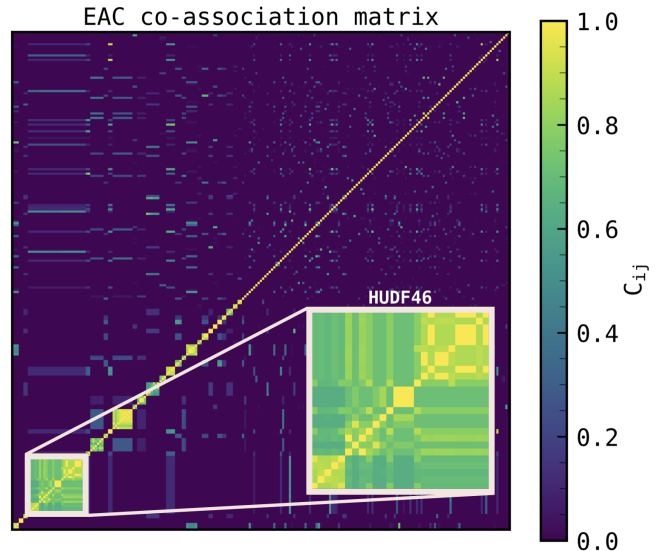


**Figure 3.** EAC co-association matrix for the HUDF spectroscopic sample. Galaxies are ordered by their final EAC consensus group for visualization only. The color scale shows the co-association value  $C_{ij}$ , i.e., the fraction of FoF realizations (across a broad grid of projected separations and velocity thresholds) in which galaxies  $i$  and  $j$  are grouped together. Diagonal elements are unity by construction. Most pairs have low  $C_{ij}$ , indicating weak association across parameter space. The highlighted region and inset zoom into HUDF46 at  $z \approx 1.84$ , revealing a compact set of galaxies consistently recovered as a group. While the visual appearance of the matrix depends on the chosen ordering, all pairwise co-association values and derived stability metrics are invariant under permutations of the axes. We note that, beyond HUDF46, other overdensities are present within HUDF, which are however less rich in member galaxies.

- *Robustness score*,  $P_{\text{score}}(i) = f_{\text{grouped}}(i) P_{\text{assoc}}(i)$ , where  $P_{\text{assoc}}$  is the 75<sup>th</sup> percentile of the  $C_{ij}$  values with  $C_{ij} \geq 0.3$ , penalizing galaxies that are either rarely grouped or lack consistently strong connections.

Finally, we classified as *secure members* those galaxies with  $P_{\text{group}} \geq 0.5$  and  $P_{\text{score}} \geq 0.5$ , i.e. objects that are both frequently recovered and tightly connected to their neighbours. This majority-rule selection is applied consistently at both the pairwise and per-galaxy level, ensuring that only statistically robust associations are retained. We visually show the result of this methodology in Figure 3.

#### 4.2. Final identification

The consensus grouping identifies the two previously reported overdensities HUDF46 at  $z \approx 1.84$  and HUDFJ0332.5–2747.3 at  $z \approx 1.89$ ; both were originally classified as proto-clusters by Mei et al. (2015) and are now expanded with additional low-mass members en-

abled by the deeper JWST data. We also identify two new overdensities at  $z \approx 1.75$  and  $z \approx 1.99$ . In what follows, we restrict our discussion to HUDF46, as it is the most prominent and best-sampled structure in our dataset, allowing a detailed characterization of both its global structure and galaxy population.

## 5. A DEEP DIVE INTO HUDF46

HUDF46 was originally identified using HST grism spectroscopy and classified as a high-redshift proto-cluster at  $z = 1.84 \pm 0.01$ , with a halo mass of  $M_{200} = (2.2 \pm 1.8) \times 10^{14} M_{\odot}$  (Mei et al. 2015). Using new JWST/NIRISS spectroscopy, we confirm HUDF46 as the richest overdensity in the NIRISS field of view at  $z \approx 1.84$ , revising its membership from 18 to 37 spectroscopically confirmed galaxies (see next section). This highlights JWST’s ability to probe the faint end of the galaxy population previously inaccessible to HST (Mei et al. 2015).

### 5.1. The final membership of HUDF46

Building on the FoF+EAC analysis presented in the previous section, we take advantage of the ultra-deep NIRISS spectroscopy to construct a richer census of HUDF46 member galaxies, down to low  $M_{\star}$  ( $\approx 10^{7.5} M_{\odot}$ ). To refine the membership of HUDF46, we applied the framework introduced by Watson et al. (2025a), which builds on established observational techniques; specifically, the modified Eisenhardt et al. (2008) method proposed by Noirot et al. (2018). This step provides the final identification of HUDF46 members used throughout the analysis.

Briefly, we made use of the secure members (QF1) to estimate an initial cluster redshift ( $z_{cl}$ ), central position (R.A., DEC), velocity dispersion ( $\sigma$ ), and  $R_{200}$  (using the formalism from Danese et al. 1980 and Carlberg et al. 1997). We then applied the method described in Watson et al. (2025a), with one key modification: instead of adopting fixed thresholds, we implemented dynamic radial and velocity cuts based on  $3 \times \sigma$  and  $3 \times R_{200}$ , assuming virialization (see next section). Cluster properties and memberships are iteratively refined using  $3\sigma$  clipping (Yahil & Vidal 1977; Blanton et al. 2000) until convergence. During this process, we also updated the central position at each step and cap the velocity dispersion at  $2000 \text{ km s}^{-1}$ , while allowing the spatial search to extend across the full NIRISS field of view.

This procedure recovers the same core members identified by the FoF+EAC method for HUDF46 and includes additional galaxies. While the core remains unchanged, the Watson et al. (2025a) approach systematically adds sources that were weakly or inconsistently

linked in the FoF runs and thus excluded by the consensus classification. This highlights the conservative nature of FoF+EAC compared to the more inclusive spatial and kinematic criteria adopted here. In total, we identify 34 members for HUDF46 (QF=1).

When cross-matching with the 18 members originally reported by Mei et al. (2015), two are excluded from our list: the first one (GMASS220) lies outside our footprint and the second one (UDF-2127) has NIRSpec confirmation at higher redshift with respect to what reported by Mei et al. (2015)<sup>6</sup>. Another object (UDF-2433), instead, lies in a crowded region dominated by very bright nearby sources. In particular, it can be cross-matched with three objects: our HUDF46+53.1472-27.7776, a passive galaxy with NIRSpec spectroscopic confirmation at  $z_{\text{NIRSpec}} = 1.6398$ , and a higher-redshift source with  $z_{\text{NIRISS}} = 1.941$ . Given the proximity of these systems and the resulting ambiguity in the association, we conservatively adopt HUDF46+53.1472-27.7776 as the most likely counterpart.

We also find that three galaxies previously assigned a quality flag QF = 3 in our NIRISS analysis exhibit redshifts (from NIRSpec) fully consistent with the HUDF46 structure; therefore we include these sources in the updated HUDF46 census, bringing the total membership to 37 galaxies. These newly identified sources have low stellar masses, with  $M_{\star} \lesssim 10^{8.5-9} M_{\odot}$ . We also identified additional potential members located outside the NIRISS footprint having NIRSpec data (for a total of 13)<sup>7</sup>, extending out to  $\approx 3 \times R_{200}$ . However, to avoid the strong incompleteness and selection biases inherent to these non-uniform NIRSpec datasets, we restrict our analysis to the uniform NIRISS-based sample. In Figure 4, we display HUDF46 members. The spectroscopically confirmed members of HUDF46 are listed in Table 1.

### 5.2. The updated properties for HUDF46

In Mei et al. (2015), the halo mass was estimated under the assumption of virialization based on multiple lines of evidence including 1) the velocity distribution of the member galaxies is gaussian, 2) an  $18\sigma$  overdensity has a high probability of being a massive node in the cosmic web rather than a filament (Hahn et al. 2007; Cautun et al. 2014), and 3) an upper limit derived using 4 Ms Chandra X-ray imaging (Xue et al. 2011) was consistent with halo masses of  $M_{200} \lesssim 10^{14} M_{\odot}$ . Such halos

<sup>6</sup> Specifically:  $z_{\text{UDF-2127, old}} = 1.858$  vs.  $z_{\text{UDF-2127, new}} = 1.863$ .

<sup>7</sup> One of these corresponds to a source reported by Mei et al. (2015) (GMASS220), previously excluded from our cross-match because it lies outside the NIRISS footprint.

**Table 1.** Spectroscopic Members of HUDF46

ID	$z_{\text{NIRISS}}$	$\log_{10}(M_{\star}/M_{\odot})$	$\mathcal{S}$	ID	$z_{\text{NIRISS}}$	$\log_{10}(M_{\star}/M_{\odot})$	$\mathcal{S}$
HUDF46+53.1541–27.7985	$1.838 \pm 0.001$	$8.71^{+0.07}_{-0.08}$	H $\beta$ , [O III], H $\alpha$	HUDF46+53.1513–27.7925*	$1.837 \pm 0.001$	$9.40^{+0.06}_{-0.03}$	H $\beta$ , [O III], H $\alpha$
HUDF46+53.1619–27.7883*	$1.840 \pm 0.001$	$8.82^{+0.05}_{-0.07}$	H $\beta$ , [O III], H $\alpha$	HUDF46+53.1609–27.7883	$1.846 \pm 0.001$	$7.84^{+0.09}_{-0.08}$	H $\beta$ , [O III], H $\alpha$
HUDF46+53.1617–27.7875* $\diamond$	$1.849 \pm 0.001$	$10.45^{+0.11}_{-0.08}$	H $\beta$ , [O III], H $\alpha$	HUDF46+53.1589–27.7858	$1.843 \pm 0.001$	$7.54^{+0.12}_{-0.14}$	H $\beta$ , [O III]
HUDF46+53.1563–27.7853	$1.840 \pm 0.002$	$7.97^{+0.12}_{-0.10}$	H $\beta$ , [O III]	HUDF46+53.1404–27.7858	$1.828 \pm 0.001$	$8.51^{+0.05}_{-0.06}$	H $\beta$ , [O III], H $\alpha$
HUDF46+53.1534–27.7811*	$1.845 \pm 0.001$	$7.50^{+0.06}_{-0.03}$	H $\beta$ , [O III], H $\alpha$	HUDF46+53.1535–27.7810*	$1.852 \pm 0.001$	$8.88^{+0.05}_{-0.03}$	H $\beta$ , [O III], H $\alpha$
HUDF46+53.1544–27.7799	$1.845 \pm 0.001$	$8.55^{+0.04}_{-0.03}$	H $\beta$ , [O III], H $\alpha$	HUDF46+53.1545–27.7798*	$1.850 \pm 0.001$	$9.57^{+0.07}_{-0.05}$	H $\alpha$
HUDF46+53.1555–27.7796*	$1.839 \pm 0.001$	$8.99^{+0.10}_{-0.07}$	H $\beta$ , [O III], H $\alpha$	HUDF46+53.1557–27.7794* $\dagger$ *	$1.845 \pm 0.001$	$10.43^{+0.07}_{-0.05}$	H $\alpha$
HUDF46+53.1529–27.7802*	$1.854 \pm 0.001$	$9.39^{+0.07}_{-0.05}$	[O II], H $\beta$ , [O III]	HUDF46+53.1492–27.7788**	$1.850 \pm 0.002$	$10.09^{+0.09}_{-0.09}$	H $\beta$ , [O III], H $\alpha$
HUDF46+53.1561–27.7760	$1.840 \pm 0.001$	$7.43^{+0.08}_{-0.07}$	H $\beta$ , [O III]	HUDF46+53.1465–27.7784*	$1.857 \pm 0.000$	$8.62^{+0.05}_{-0.06}$	H $\beta$ , [O III], H $\alpha$
HUDF46+53.1473–27.7776	$1.857 \pm 0.001$	$9.47^{+0.04}_{-0.04}$	H $\beta$ , [O III], H $\alpha$	HUDF46+53.1461–27.7781	$1.857 \pm 0.001$	$8.05^{+0.12}_{-0.19}$	H $\beta$ , [O III], H $\alpha$
HUDF46+53.1680–27.7698	$1.857 \pm 0.002$	$8.76^{+0.11}_{-0.07}$	H $\beta$ , [O III]	HUDF46+53.1600–27.7711*	$1.840 \pm 0.001$	$8.81^{+0.06}_{-0.08}$	H $\beta$ , [O III], H $\alpha$
HUDF46+53.1522–27.7732	$1.844 \pm 0.001$	$8.98^{+0.03}_{-0.16}$	H $\beta$ , [O III], H $\alpha$	HUDF46+53.1635–27.7685	$1.845 \pm 0.001$	$7.94^{+0.05}_{-0.07}$	H $\beta$ , [O III]
HUDF46+53.1529–27.7726*	$1.843 \pm 0.001$	$9.11^{+0.08}_{-0.05}$	H $\beta$ , [O III], H $\alpha$	HUDF46+53.1561–27.7710*	$1.843 \pm 0.001$	$9.42^{+0.04}_{-0.04}$	H $\beta$ , [O III], H $\alpha$
HUDF46+53.1596–27.7687	$1.843 \pm 0.001$	$7.74^{+0.15}_{-0.04}$	H $\beta$ , [O III]	HUDF46+53.1523–27.7702**	$1.840 \pm 0.005$	$9.75^{+0.06}_{-0.04}$	H $\beta$ , [O III], H $\alpha$
HUDF46+53.1647–27.7667*	$1.845 \pm 0.001$	$9.14^{+0.04}_{-0.04}$	[O II], H $\beta$ , [O III]	HUDF46+53.1393–27.7749	$1.838 \pm 0.001$	$8.55^{+0.06}_{-0.08}$	H $\beta$ , [O III], H $\alpha$
HUDF46+53.1640–27.7654*	$1.844 \pm 0.001$	$8.77^{+0.07}_{-0.09}$	H $\beta$ , [O III], H $\alpha$	HUDF46+53.1641–27.7655	$1.846 \pm 0.001$	$7.90^{+0.10}_{-0.14}$	H $\beta$ , [O III], H $\alpha$
HUDF46+53.1508–27.7692*	$1.844 \pm 0.004$	$8.57^{+0.07}_{-0.07}$	H $\beta$ , [O III], H $\alpha$	HUDF46+53.1639–27.7654*	$1.846 \pm 0.001$	$9.14^{+0.05}_{-0.07}$	H $\beta$ , [O III], H $\alpha$
HUDF46+53.1624–27.7772	$1.850 \pm 0.001$	$8.45^{+0.02}_{-0.07}$	‡	HUDF46+53.1550–27.7905	$1.849 \pm 0.001$	$8.99^{+0.06}_{-0.07}$	‡
HUDF46+53.1619–27.7683	$1.850 \pm 0.001$	$8.07^{+0.06}_{-0.07}$	‡				

NOTE— $\mathcal{S}$ : spectral features identified in NIRISS/WFSS. An asterisk (\*) refers to sources with a literature spectroscopic redshift consistent with our  $z_{\text{NIRISS}}$ . A dagger (†) marks the brightest member, located at the center of HUDF46. A double dagger (‡) identifies sources with QF = 3 (from NIRISS) confirmed by NIRSspec, typically exhibiting H $\beta$ , [O III], H $\alpha$ , and additional emission lines. Sources with \* have been recently studied in [Forrey et al. \(2025\)](#), which also have  $M_{\star}$  consistent with our measurements. Finally,  $\diamond$  marks the brightest member of HUDF46.

are expected to be largely virialized by  $z \approx 1.5$  ([Evrard et al. 2008](#)), with recent Millenium N-body simulations coupled with semi-analytic models of [Henriques et al. \(2015\)](#) predicting their gravitational collapse is largely complete by  $z \gtrsim 1.5$ , transitioning from the protocluster to the dynamically relaxed cluster phase ([Chiang et al. 2017](#); [Lim et al. 2024](#)).

Given our new, expanded membership for HUDF46, we assessed the significance of HUDF46 using the Nth-nearest neighbor technique ([Papovich et al. 2010](#); [Gobat et al. 2013](#)), as also adopted by [Mei et al. \(2015\)](#) (see our Appendix B for details). As in their study, due to the limited field of view of the NIRISS/NGDEEP observations ( $\approx 5.4 \text{ arcmin}^2$ ), we compute statistics within redshift slices over the HUDF region covered by NIRISS/WFSS, which corresponds to a co-moving size of  $\approx 1 \text{ Mpc}$  at these redshifts.

Our analysis confirms, in agreement with [Mei et al. \(2015\)](#), a significant overdensity at  $z \approx 1.84$  (HUDF46), with a contrast significance of  $\approx 17 \pm 1\sigma$  relative to the field when applying the Nth-nearest-neighbor estimator with  $N = 5-7$ . We also find a modest increase in significance at  $N = 3$  and  $N = 4$ , consistent with the densest core of the structure being probed at smaller scales. This trend likely indicates a compact and centrally concentrated galaxy distribution.

Since deeper observations have become available over time with respect to what used in [Mei et al. \(2015\)](#), we next inspected the *Chandra* data (now updated to 7 Ms). Consistent with earlier results, one galaxy in HUDF46 (HUDF46+53.1680–27.7697) coincides with X-ray source ID = 512, classified as a “galaxy without AGN” by [Xue et al. \(2011\)](#). As it was the case in [Mei et al. \(2015\)](#), no X-ray extended emission is observed even with the latest *Chandra* data, ruling out the presence of a strong/hot ICM. Nonetheless, the increased depth of the 7 Ms data allows a tighter constraint on the total halo mass, yielding an upper limit of  $M_{200} \approx (1.1-1.8) \times 10^{14} M_{\odot}$ , depending on the assumed ICM gas temperature (1–3 keV)<sup>8</sup>. These values are in good agreement with those reported by [Mei et al. \(2015\)](#). The details of our X-ray analysis are provided in Appendix C. In particular, we highlight that such values are consistent with the observed and simulated  $L_X-M_h$  relations within the associated uncertainties (e.g., [Zheng et al. 2023](#); [Nelson et al. 2024](#)).

Given these confirmations, we likewise assume HUDF46 is virialized and compute the line-of-sight velocity dispersion using the formalism of [Danese et al. \(1980\)](#)<sup>9</sup>,

<sup>8</sup> These are  $3\sigma$  upper limits.

<sup>9</sup> Which assumes that the observed redshift distribution directly traces the line-of-sight velocity spread, and thus no additional

specifically their Equations (5) and (10), and obtain  $\sigma = 670 \pm 91 \text{ km s}^{-1}$ . This value is slightly lower, though consistent within uncertainties, with the earlier estimate of  $\sigma = 730 \pm 260 \text{ km s}^{-1}$  reported by Mei et al. (2015). The reduced dispersion reflects both the increased number of members (37 vs. 18) and the improved redshift precision provided by NIRISS/WFSS.

To remain consistent with Mei et al. (2015), we first estimate the halo mass using their Equation (1), based on the calibration from Munari et al. (2013), obtaining  $M_{200} = (1.2 \pm 0.2) \times 10^{14} M_{\odot}$ . The corresponding virial radius, derived using the relation from Carlberg et al. (1997), is  $R_{200} = 0.61 \pm 0.10 \text{ Mpc}$ . Alternatively, applying the  $\sigma$ - $M_{200}$  scaling relation from Evrard et al. (2008) and adopting the spherical overdensity definition,  $R_{200} = (3M_{200}/4\pi \cdot 200 \cdot \rho_{\text{crit}}(z))^{1/3}$ , we find a slightly smaller value of  $R_{200} = 0.52 \pm 0.10 \text{ Mpc}$ , consistent with the higher critical density at this redshift. Results do not depend on using different values for  $A_{1D}$ , as pointed out also in Mei et al. (2015). In this work, we will refer to  $R_{200} = 0.61 \pm 0.10 \text{ Mpc}$  and  $M_{200} = (1.2 \pm 0.2) \times 10^{14} M_{\odot}$  to be consistent with the methods adopted in Mei et al. (2015). We warn the reader that in the case that HUDF46 is only partially or not virialized, the halo mass retrieved in this work must be considered as an upper limit.

Throughout this paper, we will refer to HUDF46 as a *young cluster*<sup>10</sup>, as it has a virial mass consistent with a gravitationally bound, cluster-scale system, while its redshift ( $z \approx 1.84$ ) and galaxy population indicate an early evolutionary stage, close to the epoch when mature clusters first emerge ( $z \lesssim 1.5$ ; e.g., Kawinwanichakij et al. 2017; Tomczak et al. 2017; Papovich et al. 2018). Therefore, the term young cluster reflects both its dynamical state and formative phase.

In Figure 5, we present our updated  $M_{200}$  measurement for HUDF46 compared with cluster and proto-cluster measurements across cosmic time ( $z \approx 0$ –5) and predictions from cosmological simulations. The simulation tracks are taken from Lim et al. (2021, 2024), who tracked the progenitors of the 25 most massive  $z = 0$  clusters in IllustrisTNG (Nelson et al. 2019) and the 100 highest-SFR haloes in FLAMINGO (Schaye et al. 2023) at each redshift snapshot. Our measured  $M_{200}$  places HUDF46 is on the simulated evolutionary tracks

correction for redshift-space distortions is applied (e.g., Ma et al. 2025).

<sup>10</sup> We remind the reader that distinctions between groups, clusters, and protoclusters are often applied pragmatically, as observational constraints rarely allow an unambiguous classification (Overzier 2016).

and firmly in the hot halo regime (Dekel & Birnboim 2006).

### 5.3. The phase-space diagram of HUDF46

Galaxies that experience environmental effects in clusters can do so on both a local or global level via multiple mechanisms. The effectiveness and timescale of these mechanisms depends on the galaxy’s infall history, which is roughly captured by probing the accretion state and orbital histories of its members in the phase-space diagram (e.g., Noble et al. 2013; Jaffé et al. 2015; Rhee et al. 2017). By combining projected clustercentric radius and line-of-sight velocity, this diagnostic retains information on time since infall. Virialized galaxies occupy the inner, low-velocity regions, while recently accreted systems lie at larger radii and higher velocities, producing the characteristic trumpet-shaped distribution (Jaffé et al. 2015; Noble et al. 2016)<sup>11</sup>.

In Figure 6, we present the projected phase-space diagram following Noble et al. (2013), where a galaxy’s position relative to the caustics traces its average infall time (commonly distinguishing ancient infallers, intermediate/backsplash galaxies, and infalling systems). We note that at this early stage, a backplash population (systems that have passed through the core and moved back to larger radii; e.g., Borrow et al. 2023) is unlikely (Hagggar et al. 2020); we therefore classify galaxies as ancient infallers, recent infallers, or ongoing infallers, the latter not necessarily bound to HUDF46.

All confirmed HUDF46 members lie within the caustic boundaries defined by Noble et al. (2016), consistent with a population dominated by ancient and recent infallers, with only one galaxy still in an active accretion phase. The brightest member is located at small projected radius and low relative velocity, consistent with a dynamically settled position near the cluster center. These objects therefore constitute a complete core sample of HUDF46, suitable for investigating early environmental processing.

We also expanded our search beyond the NIRISS footprint and identified 13 galaxies spectroscopically confirmed with NIRSpec at the redshift of HUDF46 out to  $3 \times R_{200}$ . Of these, 46% lie within the HUDF46 caustics and are thus likely gravitationally bound members. The remaining systems have less certain dynamical fates and may represent future infallers, either drawn from the surrounding field or associated with a more extended

<sup>11</sup> Although infall-time calibrations are uncertain and largely based on  $z \approx 0$  systems, phase-space diagrams remain a useful tool for interpreting the dynamical state and assembly of overdensities (e.g., Dou & Yu 2025).

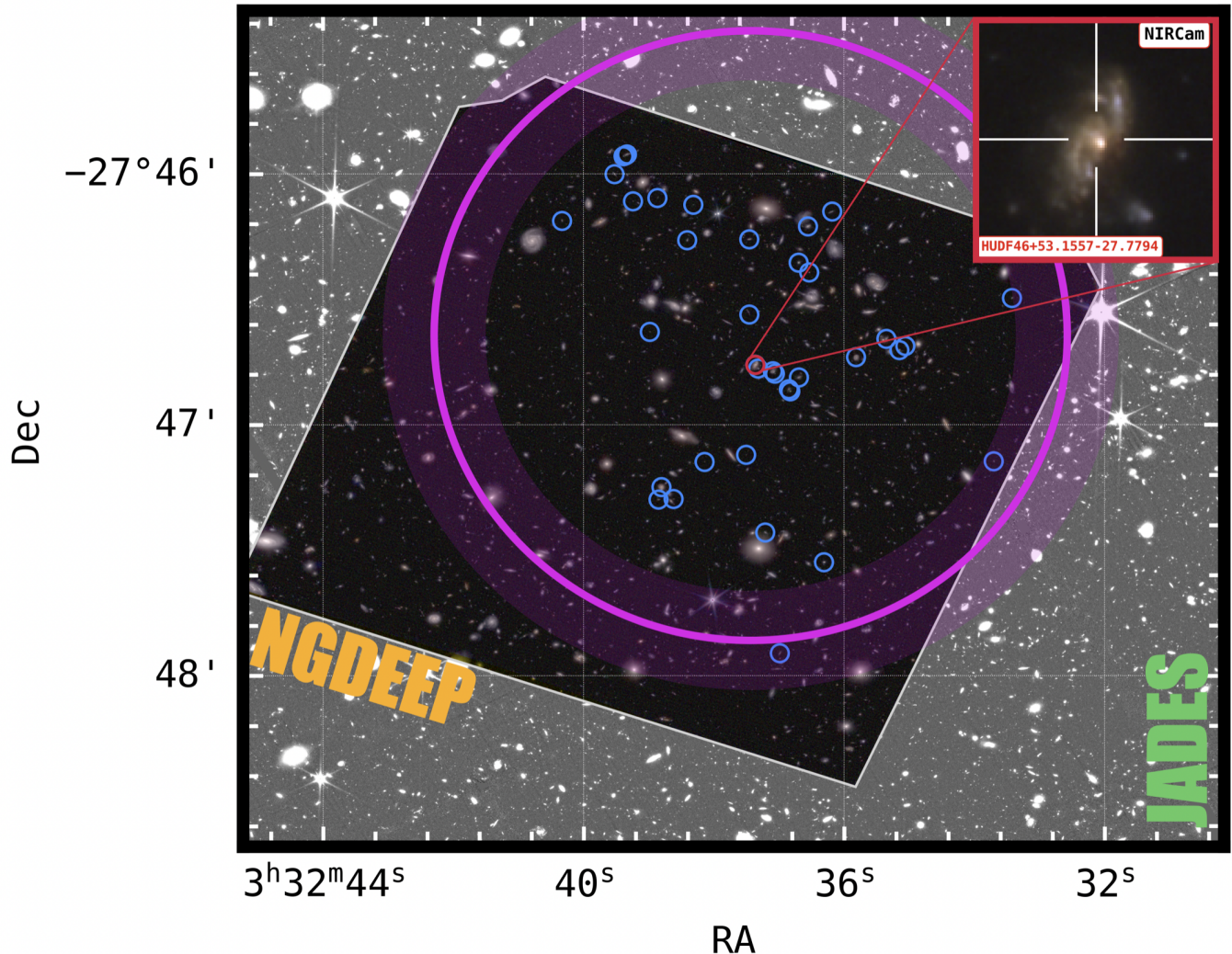


**Figure 4.** RGB image of the HUDF obtained with JWST/NIRISS (F200W, F150W, F115W), overlaid on the NIRCam/F150W grayscale mosaic from JADES. HUDF46 members are highlighted with blue circles. The virial radius,  $R_{200}$ , is shown in deep magenta, with its uncertainty indicated by the shaded region. We also show a zoom-in ( $3'' \times 3''$ ) on the brightest member (HUDF46+53.1557-27.7794), which is also the object that has been classified as an AGN according to its X-ray-to-radio luminosity ratio in Lyu et al. (2022).

proto-cluster remnant (Mei et al. 2015). We emphasize, however, that the phase-space diagram is incomplete beyond the NIRISS footprint; given this incompleteness, the present analysis focuses on the core population, deferring a detailed assessment of extended infall to future work.

In what follows, we revisit the phase-space diagram using  $\log_{10}((R/R_{200}) \times (|\Delta v|/\sigma_v))$  ( $\equiv \log_{10}(r_{\text{norm}} \times v_{\text{norm}})$ ) as an approximate proxy for infall time and relate this metric to the member-galaxy properties examined throughout the remainder of the analysis.

#### 5.4. Demographics of HUDF46

In this section, we closely examine the galaxy population within HUDF46 and compare its properties to those of field galaxies in the HUDF, in order to assess whether

systematic differences are already in place in this young cluster.

##### 5.4.1. Stellar properties of member galaxies

We used BAGPIPES (Carnall et al. 2024) to derive the stellar properties of both HUDF46 member galaxies and field galaxies. Briefly, BAGPIPES relies on synthetic templates from Bruzual & Charlot (2003) with a Kroupa (2001) IMF, adopting a cut-off mass of  $100 M_{\odot}$ , and nebular emission modeled with CLOUDY (Ferland et al. 2013). We adopted the continuity non-parametric star formation history (SFH) prior from Leja et al. (2019). For each galaxy, we defined the age bin edges (in look-back time from the redshift of observation) following a logarithmic spacing from  $z = 30$  to the age of the Universe at the corresponding redshift; the same ap-

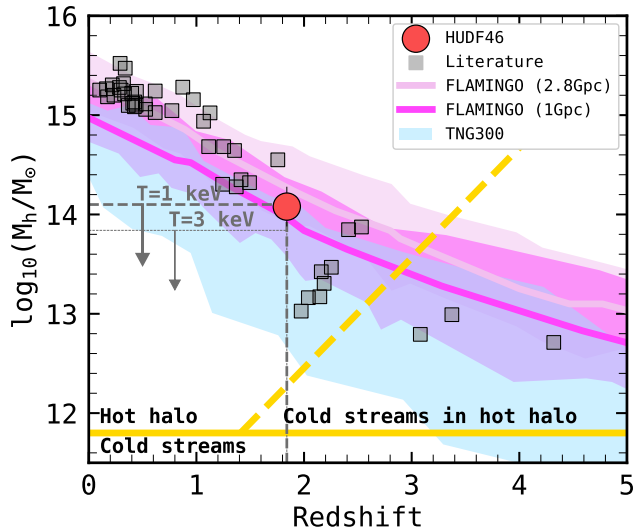


**Figure 5.** The evolution of the virial mass of haloes as a function of redshift for HUDF46 is shown alongside recent measurements at both low and high redshift (up to  $z \approx 5$ ). The observational compilation includes clusters and proto-clusters spanning  $0 \lesssim z \lesssim 5$ , such as GOODS-N (Chapman et al. 2009), MRC 1138–262 (Dannerbauer et al. 2014), SSA22 (Umehata et al. 2015), CL–J1449+0856 (Gobat et al. 2011), CL–J1001+0220 (Wang et al. 2018), PHz G237.01+42.50 (Polletta et al. 2021), CC2.2 (Darvish et al. 2020), PCL1002 (Casey et al. 2015), SPT2349–56 (Miller et al. 2018), the ISCS and SPT samples from Brodwin et al. (2011), Jee et al. (2011), and Williamson et al. (2011), as well as the massive system ACT–CL J0102–4915 (Menanteau et al. 2012). Predictions for the evolution of  $M_{200}$  as a function of cosmic time from the IllustrisTNG (Nelson et al. 2019) and FLAMINGO simulations (Schaye et al. 2023; Lim et al. 2024) are included for comparison. The derived  $M_{200}$  aligns well with the expected halo growth at  $z \approx 1.84$ . For comparison, we also show the upper limits from *Chandra* 7 Ms, assuming a blackbody ICM model with  $T = 3$  KeV and  $T = 1$  KeV. Finally, for reference, the gold dashed lines mark the different circumgalactic–gas phases defined by Dekel & Birnboim (2006).

proach was used for the age prior. Stellar masses were allowed to range from  $10^5$  to  $10^{13} M_{\odot}$ , using a uniform prior in  $\log_{10}(M_{\star}/M_{\odot})$ . We adopted a Calzetti dust attenuation law (Calzetti et al. 2000), allowing  $A_V$  to vary between 0 and 6, and set metallicity ( $Z/Z_{\odot}$ ) to vary between 0 and 2.5. The ionization parameter ( $\log_{10}(U)$ ) was allowed to vary freely between  $-4$  and  $-0.001$ . Redshifts were fixed to the spectroscopic values from NIRISS/WFSS. No AGN component was considered during the SED fitting<sup>12</sup>. In particular, the SED

<sup>12</sup> We tested whether including an AGN component for the brightest member galaxy (confirmed AGN; see next section) af-

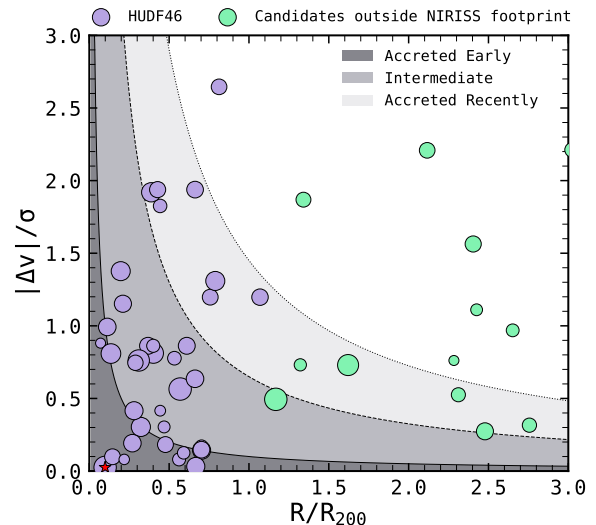


**Figure 6.** Phase–space diagram for the HUDF46 member galaxies (purple) and 13 candidate members outside the NGDEEP footprint (light gray). Point sizes scale with  $M_{\star}$ . Caustic lines follow Noble et al. (2016), adopting constant values of  $(r/r_{200}) \times (\Delta v/\sigma_v) = 0.1, 0.65,$  and  $1.45$  to delineate ancient, intermediate, and recent infallers. Nearly all confirmed HUDF46 members lie within the caustic boundaries, except for one object at  $R/R_{200} < 1$  but high  $|\Delta v|/\sigma_v$ . We retain this galaxy in the sample, noting its uncertain dynamical state. Among the candidate members, roughly half lie below the caustics at  $R/R_{200} > 1$ , with the remainder above them. The red star marks the brightest galaxy in HUDF46.

fitting is based on Kron photometry from HST/ACS, JWST/NIRCam (JADES DR2; Eisenstein et al. 2023a), and JWST/MIRI (SMILES; Alberts et al. 2024).

The SED fitting analysis shows that the HUDF46 galaxies span nearly three orders of magnitude in  $M_{\star}$ , from  $10^{7.5}$  to  $10^{10.5} M_{\odot}$ , with the majority ( $\approx 68\%$ ) lying below  $10^9 M_{\odot}$ . In contrast, only  $\approx 30\%$  of the 18 sources reported by Mei et al. (2015) had  $M_{\star} \lesssim 10^9 M_{\odot}$ . This underscores the leap forward enabled by deep NIRISS/WFSS observations in probing the low-mass end of the galaxy population in HUDF46. Compared to Mei et al. (2015), the present dataset also enables a more robust spectroscopic redshift determination, owing to the simultaneous detection of multiple emission lines, including  $H\alpha$ . We infer the stellar properties of the field galaxies ( $QF = 1$ ) using the same BAGPIPES configuration and find a similarly broad distribution in  $M_{\star}$  among the field population.

ffects the derived stellar properties, particularly  $M_{\star}$ , and find no significant differences, with all estimates consistent within  $1\sigma$ .

The HUDF46 galaxies show a wide range of dust attenuation, with  $A_V$  values spanning 0–1.5 mag, similarly to the field galaxies. The most massive systems in HUDF46 ( $M_\star \gtrsim 10^{10} M_\odot$ ), which represent only  $\approx 8\%$  of the total sample, are also the most dust-obscured, typically exhibiting  $A_V \gtrsim 1$  mag. We also find that the HUDF46 galaxies have predominantly sub-solar metallicities, consistent with the results of Shen et al. (2025), whose analysis of the same NGDEEP dataset spans a similar redshift range to that of our sample. Yet, since we do not perform spectrophotometric fitting in this work, no further constraints can be drawn.

#### 5.4.2. Does HUDF46 host AGNs?

Observationally, studies have shown that the fraction of galaxies hosting AGN increases with redshift, both in the field and in dense environments. In galaxy groups and clusters, this increase is particularly pronounced, with the AGN fraction rising rapidly toward  $z \gtrsim 1$  and in some cases exceeding field values (e.g., Martini et al. 2013; Alberts et al. 2016; Hashiguchi et al. 2023; Shah et al. 2025). For this reason, we investigated the presence of AGNs among the HUDF46 members by cross-matching with the existing pre-JWST AGN catalog of Lyu et al. (2022) (which is partly based on Luo et al. 2017), which identifies AGNs based the multi-wavelength data from the X-ray to the radio with eight independent selection methods. We found a single match: HUDF46+53.1556–27.7793, classified as an AGN because its X-ray-to-radio luminosity ratio exceeds that expected from stellar processes. Interestingly, this source is also the brightest member of HUDF46 and lies close to its center (see zoom-in in Figure 4).

We also cross-matched our sources with the recent MIRI-AGN catalog of Lyu et al. (2024), based on SMILES data, which is sensitive to lower-luminosity AGN than previous selection methods and extends to systems of lower stellar mass compared to pre-JWST catalogs. The MIRI-AGN catalog provides one additional match, but while their work lists the source at  $z = 1.98$ , our spectroscopic data place it at  $z_{\text{spec}} = 1.8574$  based on the detection of [O III] $\lambda\lambda 4959, 5007$  and  $H\beta$  emission. Given this discrepancy and the potential biases introduced by adopting an incorrect redshift during their SED fitting, we classify this source as non-AGN in our analysis<sup>13</sup>.

It is important to note that the SMILES data are relatively shallow (Alberts et al. 2024), reaching only

HUDF46 members with  $M_\star \gtrsim 10^9 M_\odot$ . As a result, 17 galaxies ( $\approx 45\%$  of the sample) are detected, while the remainder lack MIRI detection. The current MIRI-AGN catalog therefore does not allow us to fully probe the low-mass regime and assess the incidence of AGN activity in the least massive systems. However, we warn the reader that AGN identification in low-mass galaxies remains uncertain even with MIRI data (Iani et al., in prep.), as low-metallicity star-forming systems can mimic AGN-like mid-IR colors (e.g., Hainline et al. 2016). In summary, while existing catalogs rule out AGNs for all but possibly one HUDF46 member in the high-mass end, the presence of AGNs among the low-mass population cannot be fully excluded.

#### 5.4.3. Yet to quench: HUDF46 members and field galaxies aligned along the Star-Forming Main Sequence

A defining feature of galaxy clusters is the buildup of a red sequence (i.e., an excess of quenched galaxies relative to the field; e.g., De Lucia et al. 2007). While quiescent galaxies are observed in some high- $z$  proto-clusters and in clusters at  $z \approx 2$  (e.g., Sun et al. 2024; Witten et al. 2025), widespread quenching is typically established only by  $z \lesssim 1.5$  (Noordeh et al. 2021), with significant diversity during the collapse and virialization phase (Chiang et al. 2017).

In the case of HUDF46, Mei et al. (2015) found no evidence of a red sequence in their HST-selected membership. Using the catalog from Guo et al. (2013), they identified only six additional red galaxies, the brightest with spectroscopic redshifts outside the structure, confirming them as non-members. However, they cautioned, however, that some passive galaxies may lie beyond the reach of their available data, as spectroscopic confirmation is often more challenging for quiescent systems in the absence of sufficiently deep observations.

The NIRISS spectroscopy adopted in this work now doubles the number of confirmed members, enabling a reassessment of potentially missed passive systems. We reach a  $5\sigma$  1D line-flux sensitivity of  $\approx 1.3 \times 10^{-18} \text{ erg s}^{-1} \text{ cm}^{-2}$ , consistent with NGDEEP studies (Shen et al. 2024; Forrey et al. 2025; Shen et al. 2025)<sup>14</sup>, corresponding to an  $H\alpha$  star-formation rate (SFR) of  $\approx 0.17 M_\odot \text{ yr}^{-1}$  (Kennicutt & Evans 2012)<sup>15</sup>. Adopting a redshift-dependent specific SFR (sSFR) threshold of the form  $\text{sSFR}_{\text{crit}} \propto 0.2/t_H(z)$  (Pacifi et al. 2016), we

<sup>14</sup> Almost  $40\times$  deeper than HST grism observations adopted in Mei et al. (2015) in the same field.

<sup>15</sup> Note that we do not rely solely on  $H\alpha$  to identify membership; therefore,  $H\alpha$  only provides an approximate estimate of our completeness with respect to passive galaxies.

<sup>13</sup> Our visual inspection suggests that their conclusion may be driven by strong Paschen- $\alpha$  entering MIRI/F560W at that redshift, likely biasing their SED fitting results.

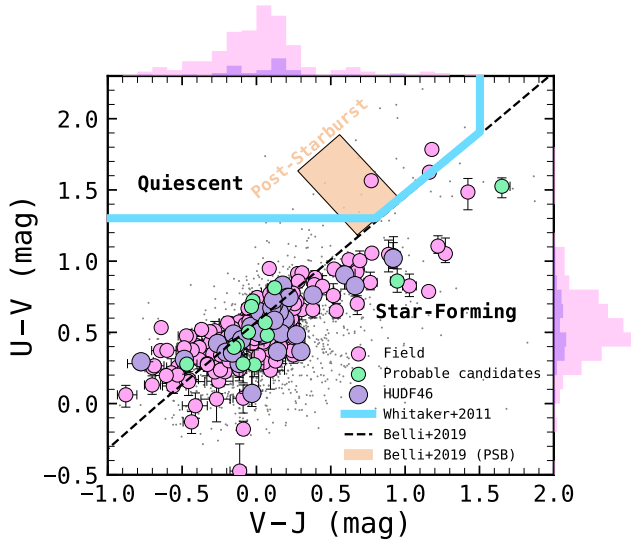


**Figure 7.** Rest-frame UVJ diagram for both field galaxies at  $z \approx 1.5\text{--}2.5$  (pink), HUDF46 (purple) members, and the JADES DR2 photometric catalog (comparable redshifts) in the HUDF (gray points; same area of NIRISS). We also show the 13 possible candidates that might belong to HUDF46 located outside the NGDEEP footprint (within  $3 \times R_{200}$ ). The solid line (turquoise blue) shows the quiescent selection of Whitaker et al. (2011), while the dashed line indicates the modified criterion of Belli et al. (2019). HUDF46 members are all consistent with the star-forming region, confirming the absence of a red sequence and in agreement with their late-type morphologies. A few members lie above the modified criterion from Belli et al. (2019), yet they show signatures of ongoing star-formation activity (through  $H\beta$ , [O III], and  $H\alpha$ ).

consider our membership to be highly complete for red galaxies down to  $M_{\star} \approx 10^{9.5} M_{\odot}$ <sup>16</sup>.

As a first attempt to look for a red sequence in HUDF46, we adopt the UVJ diagram<sup>17</sup> (Williams et al. 2009; Whitaker et al. 2011) to search for passive and post-starburst (PSB) galaxies, along with the modified criteria of Belli et al. (2019) to recover recently quenched, lower-mass systems (see Figure 7). We note that this selection has caveats: 1) by relaxing the color cuts, it can introduce contaminants and 2) it may miss some spectroscopically confirmed high- $z$  quiescent galaxies (Antwi-Danso et al. 2023; Baker et al. 2025a,b);

<sup>16</sup> Although the emission-line threshold drives our membership identification, the SFRs used throughout this paper are derived from SED fitting, not from  $H\alpha$ . Therefore, even for sources identified via [O III] with  $H\alpha$  below the detection limit, we still obtain an SFR estimate.

<sup>17</sup> UVJ magnitudes were computed with both EAZY-PY (Brammer et al. 2008) and BAGPIPES, yielding consistent results; Figure 7 shows the BAGPIPES-based colors.

however, these effects are expected to be less significant in the redshift range considered here.

We find that a few field galaxies occupy the classical quiescent region, and all are spectroscopically inconsistent with HUDF46. Some lower-mass cluster members formally satisfy the modified PSB criteria; however, their spectra show  $H\alpha$ ,  $H\beta$ , and [O III] emission, placing them on the star-forming main sequence (see next paragraphs). Given the known limitations of color-based selections and the mixed spectroscopic properties of PSBs (Nielsen et al. 2025), we conservatively flag these as PSB candidates pending further analysis.

Even with the expanded membership, HUDF46 shows no evidence for a red sequence within  $R_{200}$ , consistent with Mei et al. (2015). A search for candidates outside the NIRISS footprint (out to  $3 \times R_{200}$ ) yields no photometric candidates consistent with HUDF46 and located in the classical UVJ quenching region (Whitaker et al. 2012). This result remains tentative, as photometric redshifts can be uncertain for passive systems, and spectroscopic constraints are severely incomplete outside the NIRISS footprint.

A classical UVJ selection alone may be insufficient to robustly identify passive galaxies, though. It is often complemented by a cut in specific SFR (sSFR), adopting a redshift-dependent threshold of the form  $sSFR_{\text{crit}} \propto 0.2/t_{\text{H}(z)}$  (Pacifci et al. 2016), which corresponds to  $\approx 10^{-10.40} \text{ yr}^{-1}$  at  $z \approx 1.84$ . Therefore, as a complementary approach to the UVJ diagram, we examine the  $\text{SFR}-M_{\star}$  and  $s\text{SFR}-M_{\star}$  relations (Figure 8). From Figure 8 (left panels), we notice that nearly all HUDF46 members follow the star-forming main sequence (SFMS; Brinchmann et al. 2004; Speagle et al. 2014; Rinaldi et al. 2024), with only one clear starburst galaxy (Caputi et al. 2017; Rinaldi et al. 2022; specifically, HUDF46+53.1534–27.7811; Figure 9).

Adopting the SFMS parameterization of Leja et al. (2022), we find consistency at the high-mass end with their relation, and at low masses with its extrapolation recently derived by Mérida et al. (2025). In both the  $\text{SFR}-M_{\star}$  and  $s\text{SFR}-M_{\star}$  planes, HUDF46 and field galaxies overlap, consistent with results for massive clusters at  $z > 1$  (Alberts et al. 2016), lower-mass systems (Williams et al. 2022), and simulations from IllustrisTNG (Nelson et al. 2019; Andrews et al. 2025), which find no clear environmental dependence of the MS.

Motivated by the possibility of identifying distinct accretion histories within our sample using the projected phase-space diagram, in Figure 8 (right panels) we show

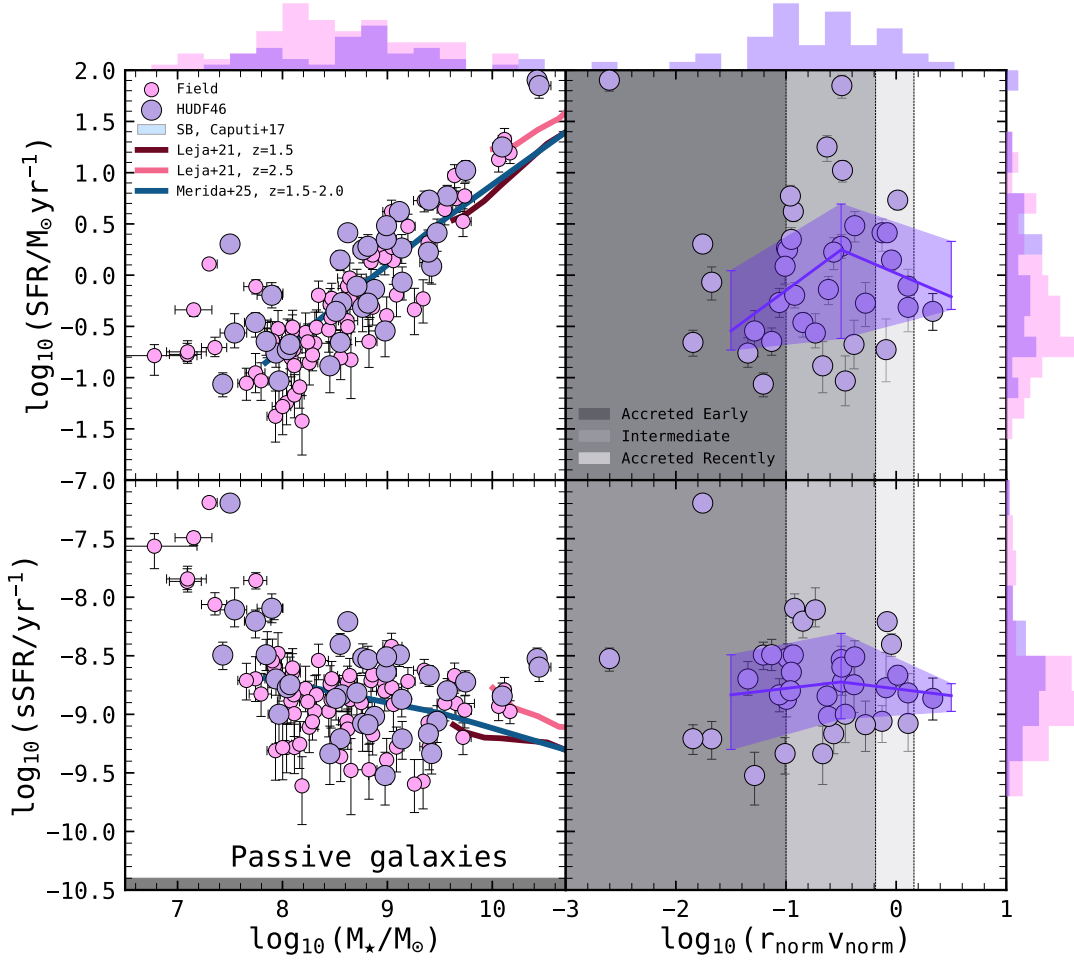


**Figure 8.** *Left:* The SFR– $M_\star$  and sSFR– $M_\star$  for both field galaxies at  $z \approx 1.7$ – $2$  (pink) and HUDF46 members (purple). For reference, we include the starburst region from Caputi et al. (2017) and the main-sequence parameterization at similar redshifts from Leja et al. (2022) and Mérida et al. (2025). In the sSFR– $M_\star$ , we also show in gray the region below which galaxies are defined as quiescent systems based on the redshift-dependent formalism from Pacifci et al. (2016), where  $\text{sSFR}_{\text{crit}} \propto 0.2/t_{\text{H}(z)}$ . On average, field and HUDF46 galaxies occupy the same locus in the SFR– $M_\star$  plane, indicating no systematic environmental differences. A few low-mass galaxies, including one HUDF46 object (HUDF46+53.1534326–27.7811176), lie significantly above the main sequence, possibly signaling a starburst episode at the time of observation. *Right:* SFR and sSFR as a function of  $\log_{10}(r_{\text{norm}} \times v_{\text{norm}})$  (following the separation adopted in Figure 6) along with the median trend. Contrary to what is commonly observed in low-redshift, more mature clusters (e.g., Noble et al. 2013, 2016), we find no substantial evolution across the accretion histories probed in HUDF46, with all members appearing overwhelmingly star-forming regardless of their orbital history.

the SFR and sSFR as a function of  $(r/r_{200}) \times (\Delta v/\sigma_v)$ <sup>18</sup> to look for slowly varying SFR and sSFR, as observed in lower-redshift clusters. Unlike low- $z$  clusters (where early infallers show suppressed star formation; Noble et al. 2013, 2016), we find no significant trend: both SFR and sSFR remain broadly flat, similar to field results (Noble et al. 2016). However, previous studies focused on more massive galaxies ( $M_\star \gtrsim 10^{9.5} M_\odot$ ) and more evolved clusters at  $z \lesssim 1.5$ , where quenching is already

advanced (Dressler 1984; Balogh et al. 2004; Kauffmann et al. 2004; Baldry et al. 2006; Muzzin et al. 2013; Kawinwanichakij et al. 2017; Tomczak et al. 2017; Papovich et al. 2018). Our results extend this into the low-mass end of the galaxy population within a cluster and it may therefore reflect either weak environmental effects in HUDF46 at Cosmic Noon or mass-dependent environmental mechanisms, as suggested by Hamadouche et al. (2025).

#### 5.4.4. Morphology of HUDF46 members

At  $z \gtrsim 1.5$ , some galaxy populations in clusters and protoclusters already show a clear morphological mix,

<sup>18</sup>  $(r/r_{200}) \times (\Delta v/\sigma_v)$  is the dimensionless phase-space coordinate tracing projected distance and velocity offset from the cluster center.

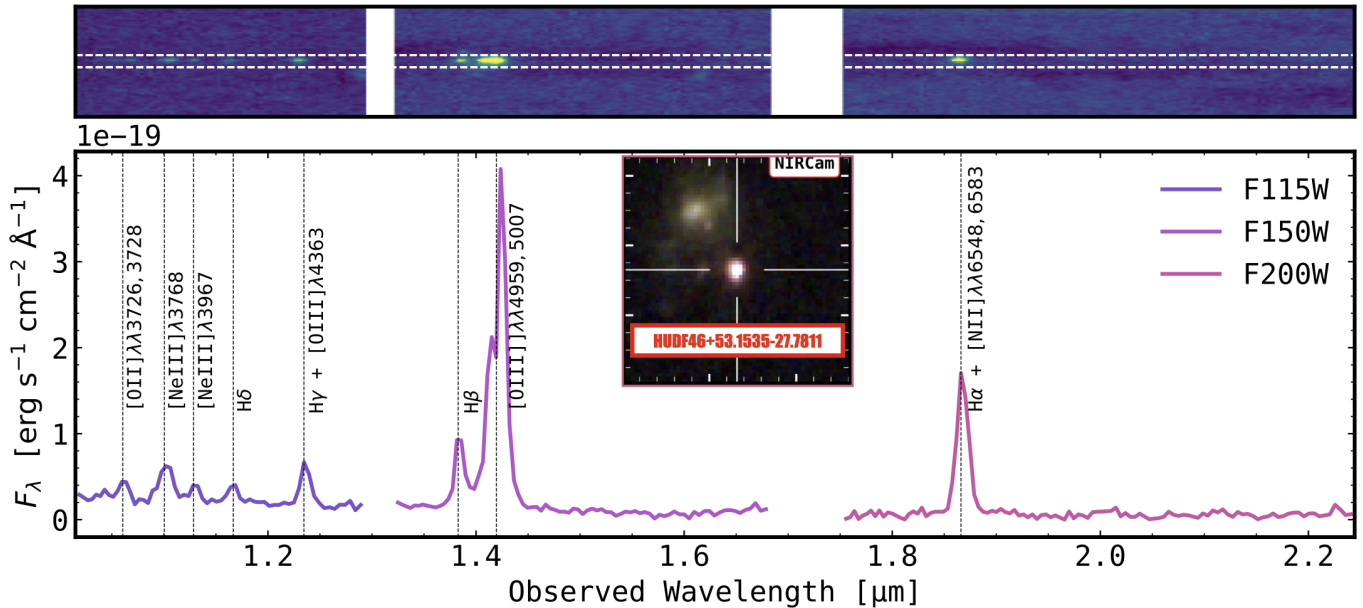


**Figure 9.** NIRISS spectrum of HUDF46+53.1534–27.7811. **Top:** continuum-subtracted 2D spectrum. **Bottom:** 1D spectrum. This is the only galaxy located in the starburst cloud (Caputi et al. 2017) of the SFR– $M_{\star}$  plane, showing multiple strong emission lines. This galaxy has  $\log_{10}(M_{\star}/M_{\odot}) = 7.89 \pm 0.15$ ,  $A_V = 0.31 \pm 0.05$  mag, a UV slope of  $\beta = -2.06 \pm 0.03$ , and  $M_{UV} = -18.55 \pm 0.05$ . Its red appearance in the NIRCcam RGB cutout (F090W, F115W, and F200W) is likely due to strong H $\alpha$  emission falling within the NIRCcam/F200W filter.

with both ETGs and late-type galaxies (LTGs) present. For instance, Mei et al. (2023) analyzed overdensities in the Clusters Around Radio-Loud AGN (CARLA) survey, which revealed that a significant fraction of galaxies display early-type morphologies even at  $z \approx 2$ , while late-type and irregular systems remain common, reflecting the ongoing assembly of these environments.

Interestingly, Mei et al. (2015) suggested that some HUDF46 members could be *star-forming* ETGs based on visual inspection. While ETGs are classically defined as morphologically early-type systems hosting old stellar populations and occupying the passive locus of the SFR– $M_{\star}$  plane in the local Universe (e.g., George & Zingade 2015), several studies have identified star-forming ETGs both locally and at intermediate redshift. In SDSS, such systems show SFRs of  $0.5\text{--}50 M_{\odot} \text{yr}^{-1}$  and often exhibit extended star formation and merger signatures (Kollmeier et al. 2025; Nolan et al. 2007; George 2017, 2023). Similarly, in  $z \approx 1\text{--}1.5$  clusters, Wagner et al. (2015) found ETGs with enhanced specific SFRs relative to local counterparts, though still below those of coeval field SFGs.

Although these findings demonstrate that an early-type morphology does not preclude ongoing star formation, recent JWST results show that deeper, higher-resolution imaging can revise morphological classifications (Ferreira et al. 2023). Using HST data, Mei et al. (2015) classified several HUDF46 members as star-forming ETGs ( $\approx 44\%$ ) of their sample). We there-

fore visually re-examined all 37 confirmed members, with particular focus on those identified as star-forming ETGs in their work.

For each source, we inspected HST and JWST imaging at comparable observed wavelengths ( $\approx 0.8\text{--}1.6 \mu\text{m}$ ) to assess potential biases arising from HST’s coarser resolution ( $0.13''/\text{px}$  for WFC3) relative to NIRCcam ( $0.031''/\text{px}$  in the short-wavelength channel). We classify galaxies as LTGs when exhibiting disks, irregular features, or clumps, and as ETGs when showing smooth, centrally concentrated light profiles. Figure 10 presents the HUDF46 members split into two stellar-mass bins, low-mass ( $M_{\star} \lesssim 10^9 M_{\odot}$ ) and high-mass ( $M_{\star} > 10^9 M_{\odot}$ ), displaying HST/WFC3 F160W and NIRCcam/F150W images, along with RGB composites from F090W, F115W, and F150W.

Our visual inspection shows that nearly all high-mass galaxies exhibit disturbed morphologies, with only one system appearing centrally concentrated. In that case, the bulge-to-total ratio ( $B/T$ ) in the NIRCcam bands is  $\approx 0.3$  (Genin et al. 2025), consistent with systems transitioning from disk- to bulge-dominated morphologies (Dimauro et al. 2022); by comparison, ETGs are typically defined by  $B/T \gtrsim 0.6$  (Dimauro et al. 2022). Among low-mass members,  $\approx 60\%$  display disturbed structures, while the remainder appear compact. Several galaxies also show clumpy or fragmented morphologies, indicative of gas-rich, gravitationally unstable disks (Zhu et al. 2026).

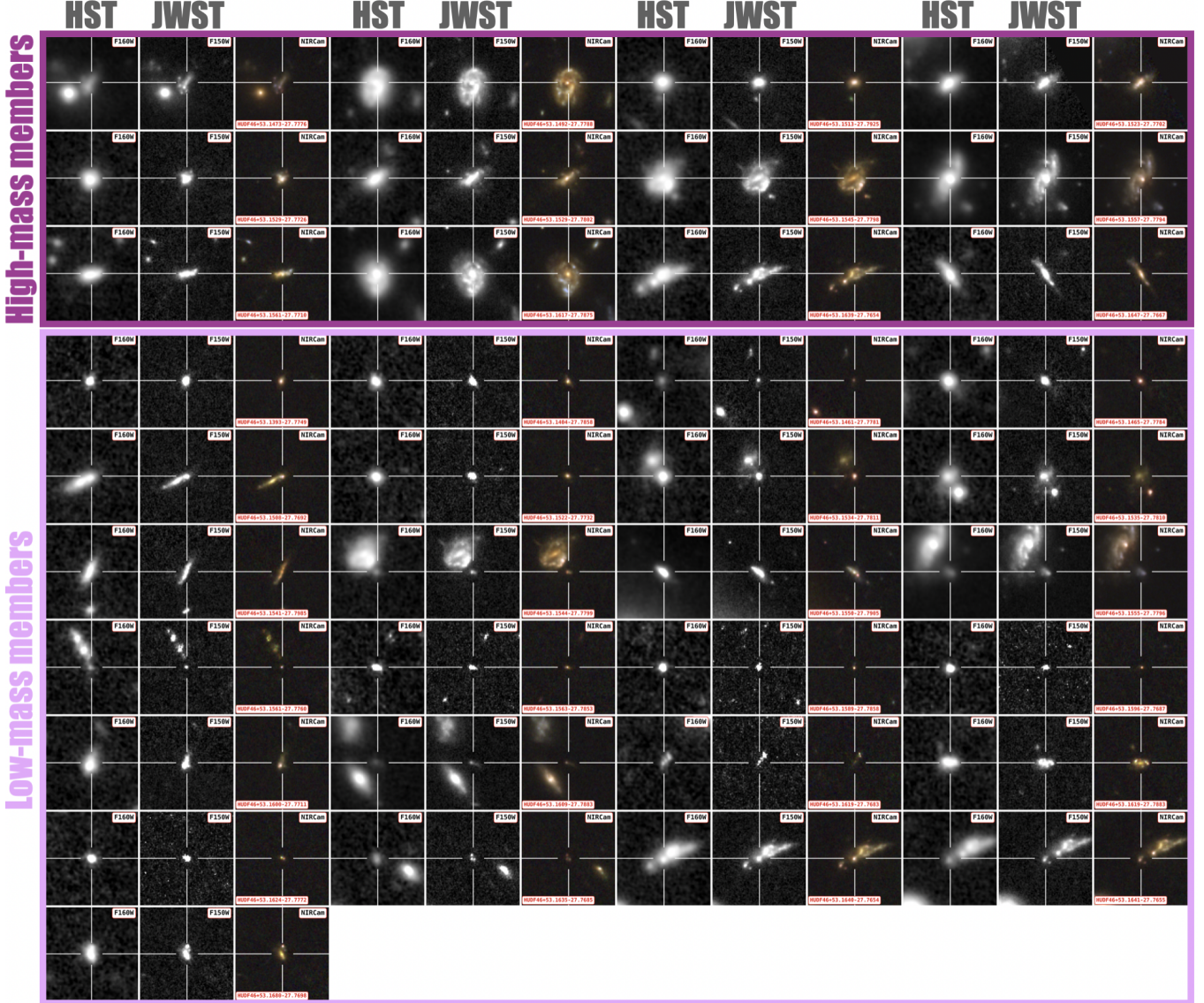


**Figure 10.** The 37 galaxies identified as HUDF46 members. For each object, we show HST/WFC3 F160W, JWST/NIRCcam F150W, and an RGB composite built from NIRCcam F090W, F115W, and F150W. Each cutout spans  $1.5'' \times 1.5''$ . The sample is divided into high-mass ( $> 10^9 M_\odot$ ) and low-mass ( $\lesssim 10^9 M_\odot$ ) galaxies. The direct comparison between HST and NIRCcam highlights how JWST’s superior sensitivity and angular resolution allow a far more reliable characterization of galaxy morphology. Several sources that appeared smooth or spheroidal in HST (potentially leading Mei et al. (2015) to classify them as ETGs) reveal clear substructure in the NIRCcam data.

Among the member galaxies, the eight systems reported as star-forming ETGs by Mei et al. (2015) warrant closer examination<sup>19</sup>. We complement our reclassification by using the morphological parameter estimates provided by Genin et al. (2025) (i.e., the bulge-to-total ratio).

<sup>19</sup> Notably, the object UDF-2383, previously reported at  $z = 1.865$ , is now confirmed by MUSE spectroscopy to lie at much lower redshift (Bacon et al. 2023).

Our JWST-based visual classifications show that none of the galaxies previously identified as star-forming ETGs display the defining morphologies of bona fide early-type systems. In all cases, the higher spatial resolution of NIRCcam reveals structures that differ markedly from the smoother HST appearance: although often compact, these galaxies are disk-dominated, irregular, asymmetric, or clumpy, and in some instances show disturbed or tidal features. Their  $B/T$  values span  $\lesssim 0.1$  to  $\approx 0.4$ , well below the  $\gtrsim 0.6$  threshold typically adopted for ETGs (e.g., Dimauro et al. 2022), confirming the absence of strongly centrally concentrated light profiles.

We therefore conclude that none of these systems can be classified as genuine ETGs. Overall, HUDF46 members show on average  $B/T \approx 0.2$  in F090W, F115W, and F150W<sup>20</sup>.

Although based on a limited sample, this comparison illustrates the step forward provided by JWST’s superior angular resolution and suggests that some HST-based classifications were affected by resolution and possibly depth limitations (see also Kuhn et al. 2024). Similar reassessments with JWST data may therefore be warranted in other structures. We conclude that, at present, there is no clear evidence for an established morphology–density relation in HUDF46.

#### 5.4.5. *The size-mass relation in HUDF46*

Over the past decades, several studies have investigated how environment can influence the structural properties of galaxies (e.g., Kuchner et al. 2017; Carlsten et al. 2021). In dense environments, environmental quenching mechanisms are expected to act preferentially on the outer regions of galaxy disks, leading to an outside-in suppression of star formation (Bluck et al. 2020). As a consequence, galaxies undergoing a transition from star-forming to quiescent phases may appear systematically more compact at fixed stellar mass, not because of an intrinsic structural transformation, but due to the fading of their outer disks (e.g., Kuchner et al. 2017). However, observational results remain mixed, with reported trends strongly dependent on sample selection, wavelength, surface-brightness limits, and morphological classification, highlighting the role of significant observational biases. For instance, recent results from, e.g., Pan et al. (2025) challenge this view, showing no significant environmental dependence in a protocluster at  $z \approx 2.6$ .

Motivated by this, we perform a similar analysis for our sample. We estimate the sizes of both field and HUDF46 galaxies using the F444W filter. In our case, the sample spans  $z \approx 1.5$ – $2.5$ , with HUDF46 members located at  $z \approx 1.84$ . At these redshifts, F444W traces rest-frame near-infrared wavelengths, providing a reliable measure of the  $M_{\star}$  distribution (Meidt et al. 2014).

Structural parameters for both field and HUDF46 galaxies are computed using PYSERSIC (Pasha & Miller 2023), a Bayesian inference framework for fitting surface brightness profiles to galaxies with robust uncertainty estimation made possible by implementing

Markov Chain Monte Carlo (MCMC) methods. The values reported here are derived from the posterior distributions of the structural parameters for single-Sérsic component fits, obtained using the MCMC sampling mode. A detailed description of the procedure for fitting Sérsic profiles to galaxies in JADES, and the resulting structural parameters, can be found in Carreira et al. (2026).

In Figure 11 (left panel), we compare the sizes of field and HUDF46 galaxies and find no significant offset between the two populations. However, three confirmed HUDF46 members lie along the lower envelope of the recent size–mass relations reported by Hamadouche et al. (2025) and show bulge-to-total ratios consistent with transitional systems ( $\approx 0.3$ – $0.4$ ) found by Genin et al. (2025). The brightest member instead lies on the upper bound of the relation from Hamadouche et al. (2025), with  $R_{\text{eff}} \approx 5$  kpc, and is the largest galaxy in the sample. The median trends in each mass bin are consistent with the results for star-forming systems reported by Hamadouche et al. (2022) and Martorano et al. (2024). When examining the sizes of HUDF46 members as a function of  $(r/r_{200}) \times (\Delta v/\sigma_v)$  (Figure 11, right panel), we find no strong trend in  $R_{\text{eff},F444W}$  across the range of inferred accretion histories, with sizes remaining approximately flat. The largest galaxy in the sample (i.e., the brightest member), however, lies in the region associated with very ancient infall, which may be consistent with its more extended structure compared to more recently accreted members.

#### 5.4.6. *No difference in Balmer/4000 Å between field and HUDF46 galaxies*

Star formation in galaxies is not eternal; it is a transient phase that can cease temporarily or permanently. When suppressed, short-lived OB stars fade and the light becomes dominated by A-type and older stars, producing a sharp feature at the Balmer limit (e.g., Bruzual A. 1983; Poggianti & Barbaro 1997). It is weak in young systems and prominent in evolved or quenched galaxies, increasing with mass-to-light ratio and decreasing with specific SFR (e.g., Worthey et al. 1994). In massive galaxies, the Balmer break is therefore commonly used as a proxy for recent quenching and assembly history. In cluster environments, its strength has been shown to depend on accretion history in massive populations, linking stellar population age to environmental processing out to intermediate redshift (e.g., Kim et al. 2023). We can now extend this analysis across the full mass range, from massive to low-mass galaxies in a young cluster, and directly compare their Balmer break strengths to those of field galaxies at similar redshift.

<sup>20</sup> Only three very compact objects, with  $M_{\star} < 10^9 M_{\odot}$ , show values above 0.4 from Genin et al. (2025); however, given their extremely small sizes, we consider these measurements likely spurious.

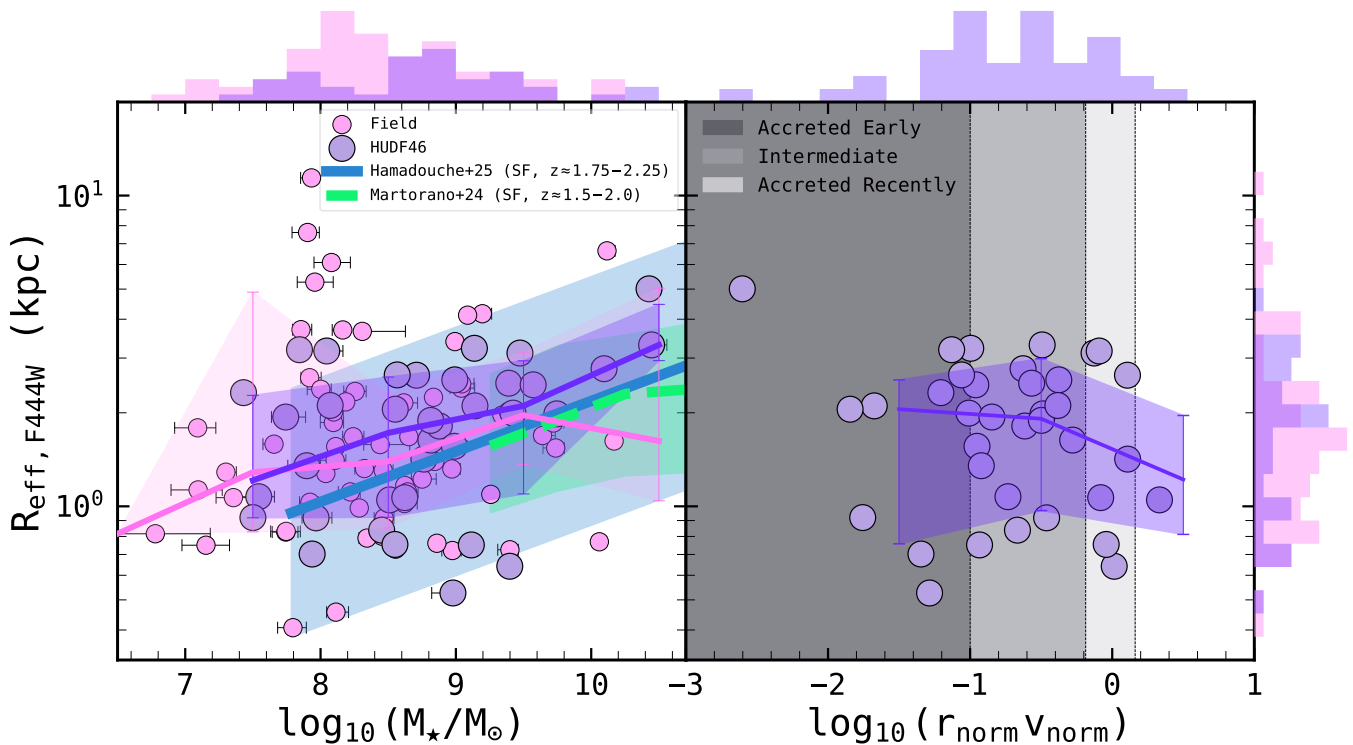


**Figure 11.** **Left:** Mass–size relation for both field galaxies at  $z \approx 1.7\text{--}2$  (pink) and HUDF46 (purple) members measured with JWST/NIRCam F444W. Median trends in stellar mass bins are shown, along with the recent size–mass relations for star-forming at comparable redshifts from Hamadouche et al. (2025) and Martorano et al. (2024). Both field and HUDF46 galaxies follow the mild evolution expected for star-forming systems, and, critically, no significant offset is detected between HUDF46 and field populations. **Right:**  $R_{\text{eff},F444W}$  as a function of  $\log_{10}(r_{\text{norm}} \times v_{\text{norm}})$  (following the separation adopted in Figure 6) along with the median trend. No substantial evolution is observed between early and recently accreted galaxies, with the median trend remaining broadly flat, although a significant diversity is present at fixed  $\log_{10}(r_{\text{norm}} \times v_{\text{norm}})$ .

Following the discussion in Wilkins et al. (2024), we quantify the break strength in field and HUDF46 member galaxies following Binggeli et al. (2019) as the more classic definition introduced by Bruzual A. (1983)<sup>21</sup> is not useful for quantifying the break in younger galaxies. Leveraging the multi-wavelength photometry and SED-fitting results, we measure the continuum in  $F_{\nu}$  at 3500 Å and 4200 Å and define  $B = F_{\nu,4200\text{Å}}/F_{\nu,3500\text{Å}}$ . This definition encompasses both the Balmer and classical 4000 Å breaks; we therefore refer to  $B$  as the Balmer/D4000 index<sup>22</sup>.

In Figure 12, we compare the Balmer/4000 Å ( $B$ ) between field and HUDF46 member galaxies. A clear stellar-mass dependence of  $B$  is observed in both environments. Figure 12 shows that there is no signifi-

cant difference in  $B$  between field galaxies and HUDF46 galaxies, especially in the low-mass regime ( $M_{\star} \lesssim 10^9 M_{\odot}$ ). One object from HUDF46 appears to exhibit a large Balmer break ( $B \approx 2.5$ ). After inspecting this source, we found that its photometry is likely contaminated by a nearby, much more massive HUDF46 member. We therefore regard this feature as spurious.

Overall, the HUDF46 members span a broad range of  $B$  values (particularly at low stellar masses) that fully overlaps with the parameter space of field galaxies. Nonetheless, as shown in Figure 8, HUDF46 galaxies lie on the star-forming main sequence, indicating ongoing star formation at the epoch of observation (with one object experiencing a pronounced starburst).

Importantly, the coexistence of relatively strong Balmer/D4000 breaks and ongoing star formation does not imply that these systems are globally quiescent. Main-sequence galaxies, particularly at low stellar masses ( $M_{\star} \lesssim 10^{8-10} M_{\odot}$ ), are expected to exhibit intrinsically bursty star formation, with variability increasing toward lower masses (Atek et al. 2022; Navarro-Carrera et al. 2024a; Simmonds et al. 2025).

<sup>21</sup> Defined as  $D_{4000}$ , which relies on using windows at [3750, 3950] Å and [4050, 4250] Å.

<sup>22</sup> We note that resolving the two components would require high-resolution spectroscopy, beyond the capabilities of the available NIRISS data given their limited spectral resolution ( $R \approx 150$ ) and wavelength coverage, which at  $z \approx 1.84$  does not fully sample the rest-frame region of interest.

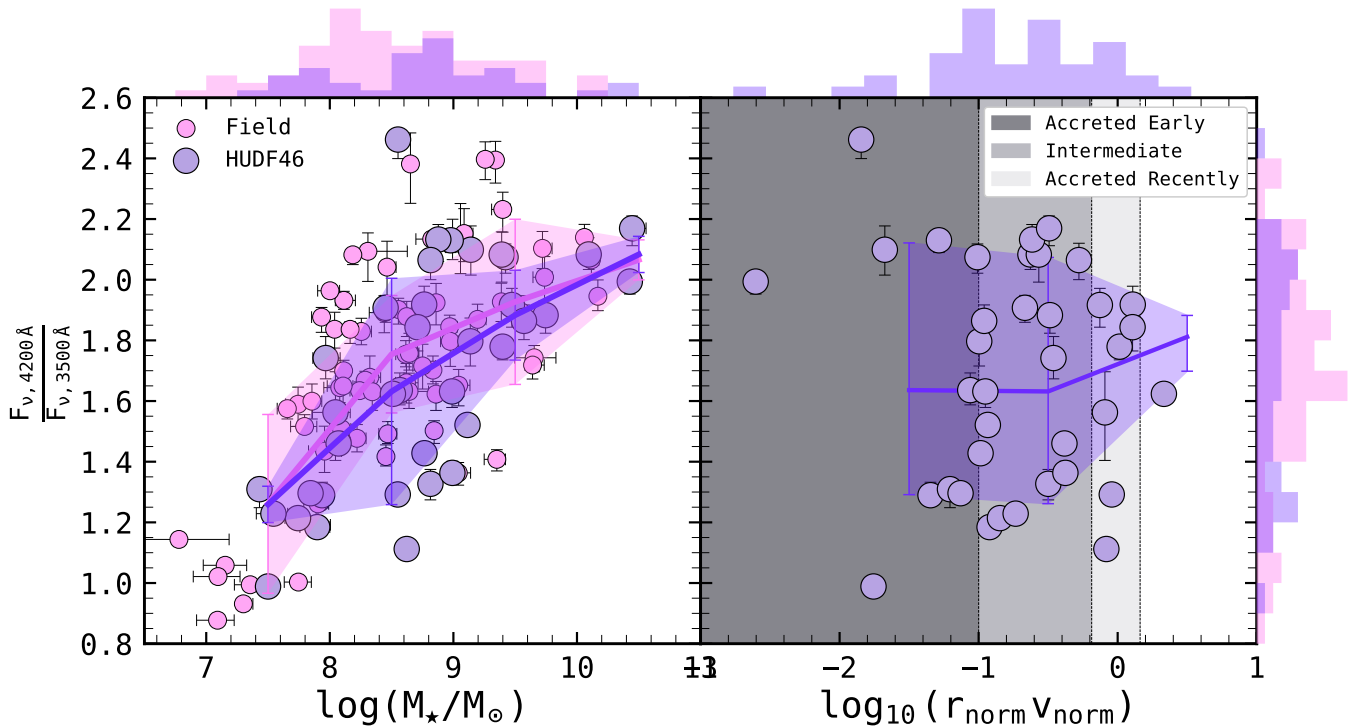


**Figure 12. Left:** The Balmer/4000 Å strength ( $B$ ) as a function of  $M_{\star}$  for both field galaxies at  $z \approx 1.7-2$  (pink) and HUDF46 (purple) members. A clear mass dependence is present, with more massive galaxies exhibiting higher  $B$  values, in line with the downsizing (Cowie et al. 1996). Notably, no systematic differences are observed between field and HUDF46 members. **Right:**  $B$  as a function of  $\log_{10}(r_{\text{norm}} \times v_{\text{norm}})$  along with the median trend. No strong variation is observed across the range of accretion histories probed in HUDF46, in clear contrast to what is typically found in more mature clusters at lower redshifts (e.g., Noble et al. 2016). On the other hand, HUDF46 members exhibit a wide spread in  $B$  at fixed  $\log_{10}(r_{\text{norm}} \times v_{\text{norm}})$ , indicating substantial diversity in their stellar populations.

In this framework, the observed  $B$  values may trace temporary lull phases between bursts rather than sustained quenching (Looser et al. 2024). At higher stellar masses, however, enhanced Balmer break/4000 Å in systems that remain consistent with the main sequence are more plausibly linked to rejuvenation episodes, frequently associated with merger-driven events at cosmic noon, which play a significant role in the buildup of the quiescent population at later times (Harrold et al. 2026).

Finally, we investigate whether  $B$  shows any dependence on accretion history by examining its behavior as a function of  $(r/r_{200}) \times (\Delta v/\sigma_v)$  in the right panel of Figure 12. In more evolved clusters at lower redshifts,  $B$  has been observed to vary systematically across phase space, decreasing monotonically toward more recent infallers (e.g., Noble et al. 2016), a trend that has also been reported in more recent work (Kim et al. 2023). In the case of HUDF46, however, we find no evidence for such a trend. Instead,  $B$  spans a wide range of values at fixed  $\log_{10}[(r/r_{200}) \times (\Delta v/\sigma_v)]$ , indicating substantial diversity among the member galaxies. As discussed earlier, this discrepancy may reflect distinct environmen-

tal quenching processes operating in low- and high-mass galaxies (e.g., Hamadouche et al. 2025).

## 6. DISCUSSION AND CONCLUSIONS

Studies of clusters and protoclusters often have to contend with biases imposed by observational limitations. (Proto)cluster selection techniques, inhomogeneous datasets, lack of spectroscopy, and restricted areal coverage can all complicate our understanding of the role of environment in galaxy evolution. Our concept and identification of galaxy clusters often hinges on the detection of an established ICM and evolved, massive populations. It is well established that the widespread quenching and morphological transformation of cluster populations is largely in place by  $z \approx 1$  (e.g., Muzzin et al. 2012; Balogh et al. 2016; Webb et al. 2013; Liu et al. 2021) and early studies projected the environmental processing of these populations back to the pre-virialized, proto-cluster phase (e.g., Thomas et al. 2005; De Lucia & Blaizot 2007). Cluster studies at  $z \approx 1-2$  have now, however, revealed substantial system-to-system variation at fixed halo mass: high-redshift clusters host both vigorously star-forming and quenched

massive galaxies (see Overzier 2016; Alberts & Noble 2022). A similar diversity is found in proto-clusters, which contain both active (e.g., Wang et al. 2016) and quenched populations (e.g., Baker et al. 2025c; Pan et al. 2025). Interpreting the protocluster to cluster transition requires a deeper look into this epoch and, particularly, the parameter space opened by JWST’s deep spectroscopic and imaging capabilities in the infrared.

### 6.1. HUDF46: a cluster in transition?

In this work, we have used ultra-deep NIRISS spectroscopy to confirm that HUDF46 is a significant overdensity ( $\delta \approx 17\sigma$ ) and measured a halo mass of  $M_{200} = (1.2 \pm 0.2) \times 10^{14} M_{\odot}$ , given the velocity distribution of its member galaxies and the assumption of virialization. This indicates that HUDF46 is a young cluster at  $z = 1.84$ , however, we have also shown that it generally lacks the hallmarks of clusters observed at later times. HUDF46 shows no signs of a red sequence, as first found in Mei et al. (2015), and the lack of X-ray detection, though consistent with the measured halo mass given its upper limit, implies a relatively weak or early stage ICM. Additionally, and puzzlingly, HUDF46 exhibits a deficit of massive ( $\gtrsim 10^{11} M_{\odot}$ ) galaxies.

At  $\log_{10}(M_h/M_{\odot}) \approx 14$ , the expected stellar mass fractions are  $M_{\star, \text{central}}/M_{\text{halo}} \approx 0.002$  and  $M_{\star, \text{total}}/M_{\text{halo}} \approx 0.01$  (e.g., Behroozi et al. 2013; Shuntov et al. 2022; Zhang et al. 2024), albeit with substantial scatter driven by galaxy properties (e.g., SFR and morphology; Zhang et al. 2024) and number density of satellites (e.g., Lu et al. 2016; Zhang et al. 2024). HUDF46 falls well below these expectations; indeed, its most massive (central) galaxy is star-forming with  $\log_{10}(M_{\star}/M_{\odot}) \approx 10.5$ , and the total stellar mass within the virial radius is only  $\log_{10}(M_{\star}/M_{\odot}) \approx 11$ , comparable to that of a typical Bright Cluster Galaxy (BCG) in a  $\log_{10}(M_h/M_{\odot}) \approx 14$  halo at much later times.

One possibility is that the assumption of full virialization is incorrect, at least in part, which would lower the inferred halo mass. However, if one were to invoke simple abundance-matching arguments, the stellar mass of HUDF46’s central galaxy would correspond to a halo mass of only  $\log_{10}(M_h/M_{\odot}) \approx 12\text{--}12.5$ . This is difficult to reconcile with its location in a  $17\sigma$  overdensity and likely fails to capture the accelerated growth expected for BCGs in dense environments at later times (e.g., DeMaio et al. 2020). Furthermore, studies of the GOGREEN clusters at  $z \approx 1\text{--}1.5$  show that the number of massive galaxies ( $\log_{10}(M_{\star}/M_{\odot}) > 10.2$ ) within 1000 kpc spans more than an order of magnitude at nearly fixed halo mass (van der Burg et al. 2020), with the low end of this distribution consistent with HUDF46.

This deficit of massive galaxies in HUDF46 may explain its lack of a quenched population, which sets HUDF46 apart from most of the clusters studied to date at  $z > 1.5$ . Often these very early clusters are reported to be evolved systems with high QG fractions<sup>23</sup> (e.g., Cooke et al. 2016; Lee-Brown et al. 2017; Newman et al. 2014; Strazzullo et al. 2019); however this excess is almost exclusively confined to the most massive galaxies ( $\gtrsim 10^{10.5\text{--}11} M_{\odot}$ ). At lower stellar masses ( $\lesssim 10^{10} M_{\odot}$ ), early cluster QG fractions are generally consistent with those of the field (e.g., Lee-Brown et al. 2017; Kiyota et al. 2025). This is consistent with the stellar-mass dependence of quenching in clusters generally seen at  $z > 1$  (e.g., Pintos-Castro et al. 2019; van der Burg et al. 2020). For the most massive cluster galaxies, multiple lines of evidence indicate they may quench predominantly through secular processes, prior to infall: their stellar ages are indistinguishable between cluster and field environments (Webb et al. 2020; Ahad et al. 2024), quenching is already evident in infall regions (Werner et al. 2022), and stellar mass functions imply early shut-down (van der Burg et al. 2020). As the HUDF itself is known to be underdense in bright sources, even compared to the broader GOODS-S field (Beckwith et al. 2006), we posit that very massive, pre-quenched galaxies were too rare in this field to fall into HUDF46 by the epoch of observation. Projecting whether HUDF46 can potentially accrete sufficient mass to approach the expected  $M_{\star}\text{--}M_h$  relation at later times, however, requires spectroscopic coverage over a *much* larger area in order to characterize the full infall population and to confirm or rule out the presence of an extended structure.

So, *is HUDF46 a cluster in transition?* With the exception of very massive galaxies, widespread quenching appears to begin in earnest around  $z \approx 1.5$  in massive clusters (Dressler 1984; Balogh et al. 2004; Kauffmann et al. 2004; Baldry et al. 2006; Muzzin et al. 2013; Alberts et al. 2014, 2016; Tomczak et al. 2017; Papovich et al. 2018). What triggers this transition is not well understood. Recently, Mei et al. (2023) showed that, for radio-selected clusters at  $z \approx 1.3\text{--}2$  from the CARLA survey Wylezalek et al. 2013, 2014; Noirod et al. 2018 with  $\log_{10}(M_h/M_{\odot}) \approx 13.5\text{--}14.5$ , the fractions of massive quenched and early-type galaxies correlate with the *local* environment rather than with global halo mass. Local studies of the effectiveness of ram pressure strip-

<sup>23</sup> This likely reflects selection biases rather than intrinsic properties, as cluster selection that relies on detection of the ICM or identifying galaxy overdensities has historically become harder with increasing redshift. This is changing in the JWST era.

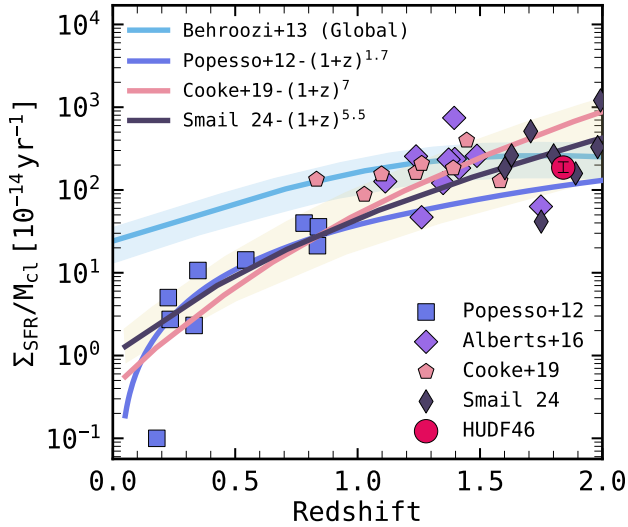


**Figure 13.** Halo mass-normalized integrated SFR as a function of redshift. We show our measurement for HUDF46 along with recent results from the literature and the derived evolution as a function of redshift from Popesso et al. (2012); Alberts et al. (2016); Cooke et al. (2019); Smail (2024). In addition, we compare to the global evolution of the mass-normalized SFR for all galaxies (sky blue line; Behroozi et al. 2013)

ping in clusters alternatively point to a threshold in the density of the ICM (Roberts et al. 2019, 2022), which could mean either globally or in terms of an individual galaxy’s trajectory after infall.

At  $z = 1.84$ , HUDF46 has been caught before this epoch of widespread quenching, potentially prior the conditions necessary to quench its population, despite its halo mass. Indeed, the system is dominated by star-forming galaxies: members lie on the star-forming main sequence, largely lack signs of post-starburst activity, and are predominantly disk-like/disturbed in morphology. With the exception of the most massive central galaxy, there is no indication of widespread AGN activity, despite some evidence that AGN fractions rise sharply with redshift in dense environments (e.g., Galametz et al. 2009; Alberts et al. 2016). The star-forming galaxies in HUDF46 are not starbursts (with the exception of one member), but instead occupy the main sequence, similarly to field galaxies at similar redshifts. Indeed, its mass-normalized cluster SFR is  $\Sigma_{\text{SFR}} = 222_{-22}^{+33} M_{\odot} \text{ yr}^{-1}$ , which corresponds to  $\Sigma_{\text{SFR}}/M_{\text{cl}} = 187_{-24}^{+32} \times 10^{-14} \text{ yr}^{-1}$  (see Figure 13); this value is consistent with theoretical expectations for protoclusters at  $z \approx 1.5\text{--}2$  (e.g., Lim et al. 2021) and there is no clear evidence for a systematic offset from

the field, consistent with the global relation of Behroozi et al. (2013).

Interestingly, recent works have shown, however, that merger-driven activity in overdensities can elevate star formation *along* the main sequence without triggering a starburst phase (e.g., Andrews et al. 2025), a scenario that is potentially consistent with the high incidence of disturbed morphologies observed among HUDF46 members, particularly at  $M_{\star} \gtrsim 10^9 M_{\odot}$ . More detailed, spatially resolved analysis is needed, however, to determine if the morphologies of HUDF46 member galaxies signal the beginnings of environmentally-driven quenching.

## 6.2. Low mass galaxies in overdense environments

Owing to observational limitations, past studies of environmentally driven galaxy evolution have largely focused on high-mass galaxies. This complicates interpretation at high redshift, as massive galaxies are rapidly quenched by secular processes, making it difficult to disentangle environmental effects. Mass and environmental quenching have been found to be largely separable down to  $\log_{10}(M_{\star}/M_{\odot}) \approx 9$  and out to  $z \approx 1$  (Peng et al. 2010, 2012); however, at  $z > 1$  the quenching of massive cluster galaxies becomes strongly mass dependent (e.g., Balogh et al. 2016; Kawinwanichakij et al. 2017; Papovich et al. 2018; Pintos-Castro et al. 2019; van der Burg et al. 2020). Dwarf galaxies, by contrast, may be intrinsically sensitive to environment. A survey of local dwarfs ( $\log_{10}(M_{\star}/M_{\odot}) < 9$ ) found that the quenched fraction in the field is extremely low, implying that nearly all quenching in dwarf galaxies occurs in overdense environments (Geha et al. 2012). This would make dwarfs the perfect laboratory for isolating environmental quenching mechanisms. Support for this picture comes from spatially resolved studies reporting outside-in quenching in dwarf galaxies (Bluck et al. 2020), although it is challenged by observational evidence for strong winds and other signatures of secular feedback (McQuinn et al. 2019).

JWST has opened a new window by pushing the stellar-mass frontier to much lower masses at all redshifts (e.g., Rinaldi et al. 2024), enabling comprehensive studies in both typical and overdense environments out to high redshift. In this work, we have used ultra-deep NIRISS spectroscopy to assemble a highly complete cluster membership spanning nearly three dex in stellar mass ( $10^{7.5\text{--}10.5} M_{\odot}$ ). Our analysis shows that essentially all confirmed members are star-forming, with a small subset potentially caught in transition toward a post-starburst phase based on their UVJ classification. We note, however, that despite pushing the membership census to very low stellar masses, the sample remains

spectroscopically incomplete for passive systems below  $\log_{10}(M_{\star}/M_{\odot}) \lesssim 9.5$ . The population spans a wide range of Balmer-break strengths, comparable to those observed in the field, and likely reflecting bursty star-formation histories (e.g., Navarro-Carrera et al. 2024b; Simmonds et al. 2025). Unlike the field, however, living in the hot halo regime (Figure 5) is expected to begin the process of starvation; a delay period is expected after infall with gas stripping becoming effective at high ICM density (Boselli et al. 2008; Roberts et al. 2019). Both cluster and local environment studies find a sharp increase in PSB and quenched low-mass galaxies at  $z < 1.5$  (Kawinwanichakij et al. 2017; McNab et al. 2021, ), which again is potentially related to reaching a threshold in the density of the ICM.

In addition to being highly susceptible to gas stripping due to their shallow potential wells (Boselli et al. 2020), low mass galaxies in overdense environments may also more strongly feel the effects of interactions and fly-bys. This again suggests an environmental role in the disturbed/irregular morphologies we observe for the HUDF46 members. Moreover, cluster members broadly follow the size–mass relation at similar redshift, with the exception of three systems ( $\log_{10}(M_{\star}/M_{\odot}) > 9$ ) that lie along its lower envelope, possibly indicating outside-in quenching and fading of their outer disks (e.g., Ito et al. 2026). As we go to lower and lower mass, however, identifying signs of interactions and spatially resolved clues like color gradients become increasingly difficult. Statistical samples of both star-forming and quenched dwarf galaxies in the extreme environments of clusters will be needed to identify trends versus the field. This input will be invaluable for dwarf galaxy models and simulations, which tend to overpredict environmental quenching at low mass (e.g., Baker et al. 2025c).

### 6.3. Summary

In this paper, we use ultra-deep JWST imaging and slitless spectroscopy to reassess the nature of the HUDF46 overdensity at  $z \approx 1.84$ . Exploiting NIRISS/WFSS spectroscopy together with NIRCам and MIRI data, we construct a highly complete spectroscopic census down to low stellar masses ( $10^{7.5} M_{\odot}$ ), almost doubling the confirmed membership relative to earlier HST-based studies (Mei et al. 2015). We derive updated dynamical properties, and characterize the stellar, structural, and star-forming properties of its galaxy population in comparison with the field. This places HUDF46 in a critical transitional phase between proto-clusters and mature clusters, prior to the onset of widespread environmental quenching. We summarize our finding below.

- New JWST data expand the HUDF46 census from 18 to 37 confirmed members (excluding two outside NGDEEP and one low- $z$  interloper), doubling the sample relative to Mei et al. (2015) while preserving a high overdensity significance of  $17 \pm 1\sigma$ .
- The expanded census allows us to revise the HUDF46 properties: we measure  $\sigma = 670 \pm 91 \text{ km s}^{-1}$ ,  $M_{200} = (1.2 \pm 0.2) \times 10^{14} M_{\odot}$ , and  $R_{200} = 0.61 \pm 0.1 \text{ Mpc}$ , all consistent with Mei et al. (2015) within uncertainties; no extended ICM emission is detected with the new *Chandra* 7 Ms data, which however set an upper limit ( $3\sigma$ ) of  $\approx (1.1\text{--}1.8) \times 10^{14} M_{\odot}$ , in line with expectations at Cosmic Noon.
- The projected phase-space distribution indicates that HUDF46 hosts a compact, gravitationally bound core dominated by already accreted galaxies. Objects beyond the NGDEEP footprint populate both the accreted and infalling regions of the phase-space diagram, consistent with ongoing assembly within the cluster-scale radii probed by the NIRISS data. We note, however, that our coverage does not extend beyond this scale, preventing a direct assessment of any larger surrounding structure.
- Using BAGPIPES, we derive stellar properties for HUDF46 and field galaxies and find no significant differences: HUDF46 spans  $M_{\star} \approx 10^{7.5}\text{--}10^{10.5} M_{\odot}$ , with 68% below  $10^9 M_{\odot}$  (a major gain over HST), shows  $A_V \approx 0\text{--}1.5 \text{ mag}$  and mostly sub-solar metallicities, and hosts at most one AGN.
- The UVJ diagram places all confirmed HUDF46 members in the star-forming region, with only a small fraction formally overlapping with the modified selection of Belli et al. (2019) to recover recently quenched, lower-mass systems, despite exhibiting clear emission lines. This classification is independently supported by their location on the SFR– $M_{\star}$  and sSFR– $M_{\star}$  main sequence. Moreover, neither SFR nor sSFR shows a systematic dependence on projected phase space, in contrast to the well-established trends observed in more mature clusters at lower redshift, indicating that environmental quenching has not yet developed in this young system.
- Revisiting morphologies with ultra-deep NIRCам, we find that the majority of HUDF46 members exhibit disk and/or disturbed morphologies—particularly at high stellar masses—while

only a small fraction appears compact. The eight star-forming ETGs previously identified by Mei et al. (2015) (with HST) instead show low bulge-to-total ratios ( $\lesssim 0.6$ ; Genin et al. 2025), consistent with disk-dominated or transitional systems (Dimauro et al. 2022). This indicates that earlier ETG classifications from Mei et al. (2015) were largely driven by resolution and depth limitations.

- We inspected the rest-frame near-IR sizes of HUDF46 and field galaxies using F444W. HUDF46 members follow a similar size–mass relation as field galaxies and are in broad agreement with the expected evolution of the relation for star-forming galaxies at similar epochs, indicating that environmental effects have not yet produced measurable structural differences at  $z \approx 1.84$ . Galaxy sizes show no systematic variation with respect to their inferred accretion history. However, the brightest member, which hosts the only AGN candidate, has  $R_{\text{eff}} \approx 5$  kpc and lies in the region associated with very ancient infall, making it a mild outlier in phase space relative to the rest of the sample.
- The Balmer/4000 Å index exhibits a clear stellar-mass dependence but shows no systematic difference between HUDF46 members and field galaxies, nor any significant trend with projected phase-space location, further indicating that environmental effects on stellar populations are not yet established in this young cluster.

This work highlights the power of deep JWST surveys to uncover structures that fall outside standard selection frameworks. At  $z \gtrsim 1.5$ –2, clusters have traditionally been identified and studied through their massive galaxy populations and/or clear signatures of maturity, such as a detectable ICM, which naturally biases the census toward already evolved systems. By contrast, studies of galaxy clusters at low redshift probe only the final stages of structure formation, after the dominant physical processes have largely concluded. The progenitors of these systems at earlier epochs must therefore exist in a much less evolved, *youthful* state; these transitional clusters can now be more readily identified and characterized through JWST’s deep near-infrared spectroscopy. In this context, HUDF46 may represent the missing link, providing a rare view of the early phases of structure assembly that eventually give rise to the massive clusters observed at much lower redshifts. In future work, we will conduct a more in-depth analysis of its population.

The authors thank Cristian Vignali for useful discussions.

This work is based on observations made with the NASA/ESA/CSA JWST. The data were obtained from the Mikulski Archive for Space Telescopes at the Space Telescope Science Institute, which is operated by the Association of Universities for Research in Astronomy, Inc., under NASA contract NAS 5-03127 for JWST. These observations are associated with JWST programs GTO #1180, GTO #1207, GO #1210, GO #1963, GO #1895, GO #2079, and # 3215. The authors acknowledge the FRESCO, JEMS, and # 3215 teams led by coPIs P. Oesch, C. C. Williams, M. Maseda, D. Eisenstein, R. Maiolino, S. Finkelstein, C. Papovich, and N. Pirzkal for developing their observing program with a zero-exclusive-access period.

Processing for the JADES NIRCcam data release was performed on the lux cluster at the University of California, Santa Cruz, funded by NSF MRI grant AST 1828315. Also based on observations made with the NASA/ESA Hubble Space Telescope obtained from the Space Telescope Science Institute, which is operated by the Association of Universities for Research in Astronomy, Inc., under NASA contract NAS 526555.

PR, CNAW, ZY and YZ acknowledge support from JWST/NIRCcam contract to the University of Arizona NAS5-02105.

PR and SA acknowledges JWST program #3432.

SA acknowledges support from the JWST Mid-Infrared Instrument (MIRI) Science Team Lead, grant 80NSSC18K0555, from NASA Goddard Space Flight Center to the University of Arizona.

WMB gratefully acknowledges support from DARK via the DARK fellowship. This work was supported by a research grant (VIL54489) from VILLUM FONDEN. GN acknowledges support by the Canadian Space Agency under a contract with NRC Herzberg Astronomy and Astrophysics.

AJB acknowledges funding from the “FirstGalaxies” Advanced Grant from the European Research Council (ERC) under the European Union’s Horizon 2020 research and innovation programme (Grant agreement No. 789056).

CC acknowledges support from the JWST/NIRCcam Science Team contract to the University of Arizona, NAS5-02105, and JWST Program 3215. JWST/NIRCcam contract to the University of Arizona, NAS5-02105.

ST acknowledges support by the Royal Society Research Grant G125142.

CJEG and LB acknowledge financial support from the Inter-University Institute for Data Intensive Astronomy (IDIA), a partnership of the University of Cape

Town, the University of Pretoria and the University of the Western Cape, and Innovation’s National Research Foundation under the ISARP RADIOMAP+ Joint Research Scheme (DSI-NRF Grant Number 150551).

LB acknowledges the financial support of the South African Department of Science and the CPRR HIPPO Project (DSI-NRF Grant Number SRUG22031677).

CJEG acknowledges the financial assistance of the South African Radio Astronomy Observatory (SARAO) ([www.sarao.ac.za](http://www.sarao.ac.za)), and the CPRR Projects (DSI-NRF Grant Number SRUG2204254729).

## APPENDIX

### A. NIRISS DATA REDUCTION

We begin from the `*_uncal.fits` exposures and run the standard `stage 1` of the `rwst pipeline` to produce `*_rate.fits` products. On these `*_rate.fits` files, we apply an additional custom striping mitigation (similar to what it is usually done with NIRC*am*; Bagley et al. 2024), generating corrected rate products that are used as input to subsequent processing. During `stage 1`, we also include an extra `column_jump` step<sup>24</sup> applied after dark current subtraction and before jump detection. This correction mitigates random column jumps (typically  $\approx 50$  per  $N_g = 100$  NISRAPID ramp) that would otherwise increase the noise. Here, “columns” refer to detector coordinates (rows in the DMS orientation), distinct from large-scale 1/f stripes.

Starting from the corrected `*_rate.fits`, we run a dedicated `stage 2` preparation to generate `*_cal.fits` products for imaging and `pseudo*_cal.fits` products for WFSS. In the latter case, we use a modified version of the GRIZLI initialization routines to apply the WCS, perform flat-fielding and WFSS background corrections, and ensure that all required GRIZLI header keywords are present for downstream spectral extraction.

The resulting `*(pseudo)cal.fits` files are used to produce mosaics for both imaging and WFSS. These mosaics serve as a baseline to construct an initial source mask, generated using SOURCE EXTRACTOR (Bertin & Arnouts 1996) and later refined using NOISECHISEL (Akhlaghi & Ichikawa 2017), which is particularly effective at detecting faint and extended emission. This mask is reprojected onto each individual exposure and used to refine background subtraction and large-scale corrections.

For imaging, the exposures are aligned to the JADES DR2 astrometric reference catalog using a modified version of the `tweakreg_step` within the `rwst pipeline`. We then run the standard `outlier_step` and `resampling_step` to produce the final mosaics, iterating the masking and background subtraction to minimize residual large-scale structures. The estimated  $5\sigma$  depths (measured in  $0.2''$  radius apertures) are 29.4 mag in F115W, 28.7 mag in F150W, and 28.7 mag in F200W, corresponding to  $\approx 0.4$ – $0.5$  mag deeper than ETC predictions. The final, background-subtracted WFSS exposures are converted into a GRIZLI-compatible `*_rate.fits` format, including a cleanup step that replaces NaNs with zeros, as expected by GRIZLI. At this stage, the imaging reduction is complete, and the WFSS products are ready for spectral extraction and analysis. Because the imaging and WFSS data have already been pre-processed with our custom NIRISS pipeline, we bypass GRIZLI’s default pre-processing and use GRIZLI directly to (i) register grism exposures to the aligned imaging, (ii) model contamination from neighboring sources, (iii) extract 2D and 1D spectra, and (iv) fit continua and emission lines. We refer the reader to Noiro*t et al.* (2023) for more details (Section 3).

### B. SIGNIFICANCE OF THE OVERDENSITIES IN HUDF

As described in Mei et al. (2015) (Section 4.1), the redshift range we focused on this work ( $z \approx 1.5 - 2.5$ ) spans different rest-frame emission lines entering and exiting the grism+filter coverage. Specifically, at  $z \lesssim 1.75$ , spectra typically contain  $H\alpha$   $\lambda 6563$ ,  $[O\text{ III}]\lambda\lambda 4959, 5007$ , and  $H\beta$   $\lambda 4861$ . By  $z \approx 2.3$ , however,  $H\alpha$  is redshifted to the red edge of the GR150+F200W range, where the throughput declines, reducing sensitivity. As a result, detections at higher redshift rely increasingly on  $[O\text{ III}]$  and  $H\beta$ , with a higher effective line-flux limit due to both weaker lines and reduced instrument sensitivity<sup>25</sup>. As noted by Mei et al. (2015), this leads to systematically lower background counts at high redshift, rendering our significance estimates at the high- $z$  end conservative.

For each overdensity, we compute projected galaxy densities using the Nth-nearest neighbor method, with  $\Sigma_N = N/(\pi D_N^2)$ , where  $N$  is the number of neighbors and  $D_N$  is the projected distance in Mpc to the Nth nearest neighbor (e.g., Dressler 1980). We evaluate  $\Sigma_N$  in redshift slices of  $\Delta z = 0.02$  between  $z = 1.5$  and  $z = 2.5$ , which balances

<sup>24</sup> Following the algorithm presented here: <https://github.com/chriswillott/jwst>

<sup>25</sup> We note that  $[O\text{ III}]\lambda\lambda 4959, 5007$  is not necessarily weaker than  $H\alpha$   $\lambda 6563$ , especially at high- $z$  (e.g., Fig. 6 in Noiro*t et al.* 2018)

sensitivity to real structures with minimal smoothing. Following [Mei et al. \(2015\)](#), the overdensity significance is defined as  $\text{SNR} = (\Sigma_N - \Sigma_N^{\text{bkg}}) / \sigma_N^{\text{bkg}}$ , where  $\Sigma_N^{\text{bkg}}$  and  $\sigma_N^{\text{bkg}}$  are the mean and standard deviation of the field distribution at a given redshift.

### C. UPDATED X-RAY MEASUREMENT FROM CHANDRA 7MS

To determine an upper limit on the X-ray luminosity of the ICM, we used the all available *Chandra* data covering the cluster, with a total exposure time of  $\approx 7$ Ms. We re-reduced and extracted the flux from all the *Chandra* observations using the Chandra Interactive Analysis of Observations (CIAO; v4.17 and CALDB 4.11.0; [Fruscione et al. 2006](#)) tools `chandra_repro` and `srcflux`. We extracted the source counts from a  $\approx 17''$  radius circular region within the previously-determined  $R_{200}$  of the cluster, in between the known X-ray sources. The background counts were extracted from a nearby source-free  $35''$  radius region. Assuming a Galactically-absorbed blackbody model for the ICM emission, with temperatures ranging between  $T = 1 - 3$  keV, we found a  $3\sigma$  upper luminosity limit of  $1.3 - 2.8 \times 10^{43}$  erg s $^{-1}$ , depending on the temperature assumed. Finally, we adopted the cluster mass-luminosity relation from [Rykoff et al. \(2008\)](#) to retrieve  $M_{200}$ .

## REFERENCES

- Ahad, S. L., Muzzin, A., Bahé, Y. M., & Hoekstra, H. 2024, *Monthly Notices of the Royal Astronomical Society*, 528, 6329. <https://ui.adsabs.harvard.edu/abs/2024MNRAS.528.6329A/abstract>
- Akhlaghi, M., & Ichikawa, T. 2017, 512, 213, conference Name: Astronomical Data Analysis Software and Systems XXV ADS Bibcode: 2017ASPC..512..213A. <https://ui.adsabs.harvard.edu/abs/2017ASPC..512..213A>
- Alberts, S., & Noble, A. 2022, *Universe*, 8, 554. <https://ui.adsabs.harvard.edu/abs/2022Univ....8..554A/abstract>
- Alberts, S., Pope, A., Brodwin, M., et al. 2014, *Monthly Notices of the Royal Astronomical Society*, 437, 437. <https://ui.adsabs.harvard.edu/abs/2014MNRAS.437.437A/abstract>
- . 2016, *The Astrophysical Journal*, 825, 72. <https://ui.adsabs.harvard.edu/abs/2016ApJ...825...72A/abstract>
- Alberts, S., Lyu, J., Shivaiei, I., et al. 2024, SMILES Initial Data Release: Unveiling the Obscured Universe with MIRI Multi-band Imaging, , publication Title: arXiv e-prints ADS Bibcode: 2024arXiv240515972A, doi:10.48550/arXiv.2405.15972. <https://ui.adsabs.harvard.edu/abs/2024arXiv240515972A>
- Andrews, M., Artale, M. C., Kumar, A., et al. 2025, *Astronomy and Astrophysics*, 698, A280. <https://ui.adsabs.harvard.edu/abs/2025A&A...698A.280A/abstract>
- Antwi-Danso, J., Papovich, C., Leja, J., et al. 2023, *The Astrophysical Journal*, 943, 166. <https://ui.adsabs.harvard.edu/abs/2023ApJ...943..166A/abstract>
- Atek, H., Furtak, L. J., Oesch, P., et al. 2022, *Monthly Notices of the Royal Astronomical Society*, 511, 4464, aDS Bibcode: 2022MNRAS.511.4464A. <https://ui.adsabs.harvard.edu/abs/2022MNRAS.511.4464A>
- Bacon, R., Brinchmann, J., Conseil, S., et al. 2023, *Astronomy and Astrophysics*, 670, A4. <https://ui.adsabs.harvard.edu/abs/2023A&A...670A...4B/abstract>
- Bagley, M. B., Pirzkal, N., Finkelstein, S. L., et al. 2024, *The Astrophysical Journal*, 965, L6, aDS Bibcode: 2024ApJ...965L...6B. <https://ui.adsabs.harvard.edu/abs/2024ApJ...965L...6B>
- Baker, W. M., Lim, S., D'Eugenio, F., et al. 2025a, *Monthly Notices of the Royal Astronomical Society*, 539, 557. <https://ui.adsabs.harvard.edu/abs/2025MNRAS.539..557B/abstract>
- Baker, W. M., Valentino, F., Lagos, C. d. P., et al. 2025b, *Astronomy and Astrophysics*, 702, A270. <https://ui.adsabs.harvard.edu/abs/2025A&A...702A.270B/abstract>
- Baker, W. M., Ito, K., Valentino, F., et al. 2025c, arXiv e-prints, arXiv:2509.09761. <https://ui.adsabs.harvard.edu/abs/2025arXiv250909761B/abstract>
- Baldry, I. K., Balogh, M. L., Bower, R. G., et al. 2006, *Monthly Notices of the Royal Astronomical Society*, 373, 469. <https://ui.adsabs.harvard.edu/abs/2006MNRAS.373..469B/abstract>
- Balogh, M. L., Baldry, I. K., Nichol, R., et al. 2004, *The Astrophysical Journal*, 615, L101. <https://ui.adsabs.harvard.edu/abs/2004ApJ...615L.101B/abstract>
- Balogh, M. L., McGee, S. L., Mok, A., et al. 2016, *Monthly Notices of the Royal Astronomical Society*, 456, 4364. <https://ui.adsabs.harvard.edu/abs/2016MNRAS.456.4364B/abstract>
- Beckwith, S. V. W., Stiavelli, M., Koekemoer, A. M., et al. 2006, *The Astrophysical Journal*, 132, 1729. <https://ui.adsabs.harvard.edu/abs/2006AJ....132.1729B/abstract>
- Behroozi, P. S., Wechsler, R. H., & Conroy, C. 2013, *The Astrophysical Journal*, 770, 57. <https://ui.adsabs.harvard.edu/abs/2013ApJ...770...57B/abstract>
- Belli, S., Newman, A. B., & Ellis, R. S. 2019, *The Astrophysical Journal*, 874, 17. <https://ui.adsabs.harvard.edu/abs/2019ApJ...874...17B/abstract>
- Berlind, A. A., Frieman, J., Weinberg, D. H., et al. 2006, *The Astrophysical Journal Supplement Series*, 167, 1. <https://ui.adsabs.harvard.edu/abs/2006ApJS..167....1B/abstract>
- Berrier, J. C., Stewart, K. R., Bullock, J. S., et al. 2009, *The Astrophysical Journal*, 690, 1292. <https://ui.adsabs.harvard.edu/abs/2009ApJ...690.1292B/abstract>
- Bertin, E., & Arnouts, S. 1996, *Astronomy and Astrophysics Supplement Series*, 117, 393, aDS Bibcode: 1996A&AS..117..393B. <https://ui.adsabs.harvard.edu/abs/1996A&AS..117..393B>
- Binggeli, C., Zackrisson, E., Ma, X., et al. 2019, *Monthly Notices of the Royal Astronomical Society*, 489, 3827. <https://ui.adsabs.harvard.edu/abs/2019MNRAS.489.3827B/abstract>
- Birkinshaw, M. 1999, *Physics Reports*, 310, 97. <https://ui.adsabs.harvard.edu/abs/1999PhR...310...97B/abstract>
- Birnboim, Y., & Dekel, A. 2003, *Monthly Notices of the Royal Astronomical Society*, 345, 349. <https://ui.adsabs.harvard.edu/abs/2003MNRAS.345..349B/abstract>
- Blanton, E. L., Gregg, M. D., Helfand, D. J., Becker, R. H., & White, R. L. 2000, *The Astrophysical Journal*, 531, 118. <https://ui.adsabs.harvard.edu/abs/2000ApJ...531..118B/abstract>
- Blanton, M. R., & Moustakas, J. 2009, *Annual Review of Astronomy and Astrophysics*, 47, 159. <https://ui.adsabs.harvard.edu/abs/2009ARA&A..47..159B/abstract>

- Bluck, A. F. L., Maiolino, R., Piotrowska, J. M., et al. 2020, *Monthly Notices of the Royal Astronomical Society*, 499, 230. <https://ui.adsabs.harvard.edu/abs/2020MNRAS.499..230B/abstract>
- Borrow, J., Vogelsberger, M., O’Neil, S., McDonald, M. A., & Smith, A. 2023, *Monthly Notices of the Royal Astronomical Society*, 520, 649. <https://ui.adsabs.harvard.edu/abs/2023MNRAS.520..649B/abstract>
- Boselli, A., Boissier, S., Cortese, L., & Gavazzi, G. 2008, *The Astrophysical Journal*, 674, 742. <https://ui.adsabs.harvard.edu/abs/2008ApJ...674..742B/abstract>
- Boselli, A., & Gavazzi, G. 2006, *Publications of the Astronomical Society of the Pacific*, 118, 517. <https://ui.adsabs.harvard.edu/abs/2006PASP..118..517B/abstract>
- Boselli, A., Voyer, E., Boissier, S., et al. 2014, *Astronomy and Astrophysics*, 570, A69. <https://ui.adsabs.harvard.edu/abs/2014A&A...570A..69B/abstract>
- Boselli, A., Fossati, M., Longobardi, A., et al. 2020, *Astronomy and Astrophysics*, 634, L1. <https://ui.adsabs.harvard.edu/abs/2020A&A...634L...1B/abstract>
- Brammer, G., & Matharu, J. 2021, Zenodo, doi:10.5281/zenodo.5012699, aDS Bibcode: 2021zndo...5012699B. <https://ui.adsabs.harvard.edu/abs/2021zndo...5012699B>
- Brammer, G. B., van Dokkum, P. G., & Coppi, P. 2008, *The Astrophysical Journal*, 686, 1503. <https://ui.adsabs.harvard.edu/abs/2008ApJ...686.1503B/abstract>
- Brammer, G. B., van Dokkum, P. G., Franx, M., et al. 2012, *The Astrophysical Journal Supplement Series*, 200, 13, aDS Bibcode: 2012ApJS..200...13B. <https://ui.adsabs.harvard.edu/abs/2012ApJS..200...13B>
- Brinchmann, J., Charlot, S., White, S. D. M., et al. 2004, *Monthly Notices of the Royal Astronomical Society*, 351, 1151. <https://ui.adsabs.harvard.edu/abs/2004MNRAS.351.1151B/abstract>
- Brodwin, M., Stern, D., Vikhlinin, A., et al. 2011, *The Astrophysical Journal*, 732, 33. <https://ui.adsabs.harvard.edu/abs/2011ApJ...732...33B/abstract>
- Bruzual, G., & Charlot, S. 2003, *Monthly Notices of the Royal Astronomical Society*, 344, 1000, aDS Bibcode: 2003MNRAS.344.1000B. <https://ui.adsabs.harvard.edu/abs/2003MNRAS.344.1000B>
- Bruzual A., G. 1983, *The Astrophysical Journal*, 273, 105. <https://ui.adsabs.harvard.edu/abs/1983ApJ...273..105B/abstract>
- Butcher, H., & Oemler, A. 1978, *The Astrophysical Journal*, 219, 18. <https://ui.adsabs.harvard.edu/abs/1978ApJ...219...18B/abstract>
- Calzetti, D., Armus, L., Bohlin, R. C., et al. 2000, *The Astrophysical Journal*, 533, 682, aDS Bibcode: 2000ApJ...533..682C. <https://ui.adsabs.harvard.edu/abs/2000ApJ...533..682C>
- Caputi, K. I., Deshmukh, S., Ashby, M. L. N., et al. 2017, *The Astrophysical Journal*, 849, 45, aDS Bibcode: 2017ApJ...849...45C. <https://ui.adsabs.harvard.edu/abs/2017ApJ...849...45C>
- Caputi, K. I., Rinaldi, P., Iani, E., et al. 2024, *The Astrophysical Journal*, 969, 159, aDS Bibcode: 2024ApJ...969..159C. <https://ui.adsabs.harvard.edu/abs/2024ApJ...969..159C>
- Carlberg, R. G., Yee, H. K. C., & Ellingson, E. 1997, *The Astrophysical Journal*, 478, 462. <https://ui.adsabs.harvard.edu/abs/1997ApJ...478..462C/abstract>
- Carlsten, S. G., Greene, J. E., Greco, J. P., Beaton, R. L., & Kado-Fong, E. 2021, *The Astrophysical Journal*, 922, 267. <https://ui.adsabs.harvard.edu/abs/2021ApJ...922..267C/abstract>
- Carnall, A. C., Cullen, F., McLure, R. J., et al. 2024, *Monthly Notices of the Royal Astronomical Society*, 534, 325. <https://ui.adsabs.harvard.edu/abs/2024MNRAS.534..325C/abstract>
- Carreira, C., Robertson, B. E., Danhaive, A. L., et al. 2026, arXiv e-prints, arXiv:2601.15957. <https://ui.adsabs.harvard.edu/abs/2026arXiv260115957C/abstract>
- Casey, C. M., Cooray, A., Capak, P., et al. 2015, *The Astrophysical Journal*, 808, L33. <https://ui.adsabs.harvard.edu/abs/2015ApJ...808L..33C/abstract>
- Cautun, M., Hellwing, W. A., van de Weygaert, R., et al. 2014, *Monthly Notices of the Royal Astronomical Society*, 445, 1820. <https://ui.adsabs.harvard.edu/abs/2014MNRAS.445.1820C/abstract>
- Chapman, S. C., Blain, A., Ibata, R., et al. 2009, *The Astrophysical Journal*, 691, 560. <https://ui.adsabs.harvard.edu/abs/2009ApJ...691..560C/abstract>
- Chiang, Y.-K., Overzier, R. A., Gebhardt, K., & Henriques, B. 2017, *The Astrophysical Journal*, 844, L23. <https://ui.adsabs.harvard.edu/abs/2017ApJ...844L..23C/abstract>
- Conroy, C., & Gunn, J. E. 2010, *Astrophysics Source Code Library*, ascl:1010.043, aDS Bibcode: 2010ascl.soft10043C. <https://ui.adsabs.harvard.edu/abs/2010ascl.soft10043C>
- Cooke, E. A., Smail, I., Stach, S. M., et al. 2019, *Monthly Notices of the Royal Astronomical Society*, 486, 3047. <https://ui.adsabs.harvard.edu/abs/2019MNRAS.486.3047C/abstract>
- Cooke, E. A., Hatch, N. A., Stern, D., et al. 2016, *The Astrophysical Journal*, 816, 83. <https://ui.adsabs.harvard.edu/abs/2016ApJ...816...83C/abstract>

- Courtin, J., Rasera, Y., Alimi, J.-M., et al. 2011, *Monthly Notices of the Royal Astronomical Society*, 410, 1911. <https://ui.adsabs.harvard.edu/abs/2011MNRAS.410.1911C/abstract>
- Cowie, L. L., Songaila, A., Hu, E. M., & Cohen, J. G. 1996, *The Astronomical Journal*, 112, 839. <https://ui.adsabs.harvard.edu/abs/1996AJ....112..839C/abstract>
- Croton, D. J., Springel, V., White, S. D. M., et al. 2006, *Monthly Notices of the Royal Astronomical Society*, 365, 11. <https://ui.adsabs.harvard.edu/abs/2006MNRAS.365..11C/abstract>
- Cutler, S. E., Weaver, J. R., Whitaker, K. E., et al. 2025, *The Astrophysical Journal*, 993, 169. <https://ui.adsabs.harvard.edu/abs/2025ApJ...993..169C/abstract>
- Danese, L., de Zotti, G., & di Tullio, G. 1980, *Astronomy and Astrophysics*, 82, 322. <https://ui.adsabs.harvard.edu/abs/1980A&A....82..322D/abstract>
- Dannerbauer, H., Kurk, J. D., De Breuck, C., et al. 2014, *Astronomy and Astrophysics*, 570, A55. <https://ui.adsabs.harvard.edu/abs/2014A&A...570A..55D/abstract>
- Darvish, B., Mobasher, B., Sobral, D., Scoville, N., & Aragon-Calvo, M. 2015, *The Astrophysical Journal*, 805, 121. <https://ui.adsabs.harvard.edu/abs/2015ApJ...805..121D/abstract>
- Darvish, B., Scoville, N. Z., Martin, C., et al. 2020, *The Astrophysical Journal*, 892, 8. <https://ui.adsabs.harvard.edu/abs/2020ApJ...892....8D/abstract>
- De Lucia, G., & Blaizot, J. 2007, *Monthly Notices of the Royal Astronomical Society*, 375, 2. <https://ui.adsabs.harvard.edu/abs/2007MNRAS.375....2D/abstract>
- De Lucia, G., Poggianti, B. M., Aragón-Salamanca, A., et al. 2007, *Monthly Notices of the Royal Astronomical Society*, 374, 809. <https://ui.adsabs.harvard.edu/abs/2007MNRAS.374..809D/abstract>
- Dekel, A., & Birnboim, Y. 2006, *Monthly Notices of the Royal Astronomical Society*, 368, 2. <https://ui.adsabs.harvard.edu/abs/2006MNRAS.368....2D/abstract>
- DeMaio, T., Gonzalez, A. H., Zabludoff, A., et al. 2020, *Monthly Notices of the Royal Astronomical Society*, 491, 3751. <https://ui.adsabs.harvard.edu/abs/2020MNRAS.491.3751D/abstract>
- D'Eugenio, F., Cameron, A. J., Scholtz, J., et al. 2024, *JADES Data Release 3 – NIRSpec/MSA spectroscopy for 4,000 galaxies in the GOODS fields*, , , publication Title: arXiv e-prints ADS Bibcode: 2024arXiv240406531D, doi:10.48550/arXiv.2404.06531. <https://ui.adsabs.harvard.edu/abs/2024arXiv240406531D>
- Dimauro, P., Daddi, E., Shankar, F., et al. 2022, *Monthly Notices of the Royal Astronomical Society*, 513, 256. <https://ui.adsabs.harvard.edu/abs/2022MNRAS.513..256D/abstract>
- Dou, H., & Yu, H. 2025, *Astronomy and Astrophysics*, 699, A95. <https://ui.adsabs.harvard.edu/abs/2025A&A...699A..95D/abstract>
- Doyon, R., Willott, C. J., Hutchings, J. B., et al. 2023, *Publications of the Astronomical Society of the Pacific*, 135, 098001. <https://ui.adsabs.harvard.edu/abs/2023PASP..135i8001D/abstract>
- Dressler, A. 1980, *Astrophysical Journal*, Vol. 236, p. 351-365 (1980), 236, 351. <https://ui.adsabs.harvard.edu/abs/1980ApJ...236..351D/abstract>
- . 1984, *Annual Review of Astronomy and Astrophysics*, 22, 185. <https://ui.adsabs.harvard.edu/abs/1984ARA&A..22..185D/abstract>
- Eisenhardt, P. R. M., Brodwin, M., Gonzalez, A. H., et al. 2008, *The Astrophysical Journal*, 684, 905. <https://ui.adsabs.harvard.edu/abs/2008ApJ...684..905E/abstract>
- Eisenstein, D. J., Johnson, B. D., Robertson, B., et al. 2023a, *The JADES Origins Field: A New JWST Deep Field in the JADES Second NIRCcam Data Release*, , , publication Title: arXiv e-prints ADS Bibcode: 2023arXiv231012340E, doi:10.48550/arXiv.2310.12340. <https://ui.adsabs.harvard.edu/abs/2023arXiv231012340E>
- Eisenstein, D. J., Willott, C., Alberts, S., et al. 2023b, *Overview of the JWST Advanced Deep Extragalactic Survey (JADES)*, , , publication Title: arXiv e-prints ADS Bibcode: 2023arXiv230602465E, doi:10.48550/arXiv.2306.02465. <https://ui.adsabs.harvard.edu/abs/2023arXiv230602465E>
- Evrard, A. E., Bialek, J., Busha, M., et al. 2008, *The Astrophysical Journal*, 672, 122. <https://ui.adsabs.harvard.edu/abs/2008ApJ...672..122E/abstract>
- Ferland, G. J., Porter, R. L., van Hoof, P. A. M., et al. 2013, *Revista Mexicana de Astronomia y Astrofisica*, 49, 137, aDS Bibcode: 2013RMxAA..49..137F. <https://ui.adsabs.harvard.edu/abs/2013RMxAA..49..137F>
- Ferreira, L., Conselice, C. J., Sazonova, E., et al. 2023, *The Astrophysical Journal*, 955, 94. <https://ui.adsabs.harvard.edu/abs/2023ApJ...955...94F/abstract>
- Ferruit, P., Jakobsen, P., Giardino, G., et al. 2022, *Astronomy and Astrophysics*, 661, A81, aDS Bibcode: 2022A&A...661A..81F. <https://ui.adsabs.harvard.edu/abs/2022A&A...661A..81F>
- Foley, R. J., Andersson, K., Bazin, G., et al. 2011, *The Astrophysical Journal*, 731, 86. <https://ui.adsabs.harvard.edu/abs/2011ApJ...731...86F/abstract>

- Forrey, G. M., Simons, R. C., Trump, J. R., et al. 2025, arXiv e-prints, arXiv:2512.11989. <https://ui.adsabs.harvard.edu/abs/2025arXiv251211989F/abstract>
- Fred, A. L. N., & Jain, A. K. 2005, *IEEE Transactions on Pattern Analysis and Machine Intelligence*, 27, 835. <https://ui.adsabs.harvard.edu/abs/2005ITPAM..27..835F/abstract>
- Fruscione, A., McDowell, J. C., Allen, G. E., et al. 2006, *Observatory Operations: Strategies, Processes, and Systems*, 6270, 62701V. <https://ui.adsabs.harvard.edu/abs/2006SPIE.6270E..1VF/abstract>
- Fudamoto, Y., Helton, J. M., Lin, X., et al. 2025, arXiv e-prints, arXiv:2503.15597. <https://ui.adsabs.harvard.edu/abs/2025arXiv250315597F/abstract>
- Galametz, A., Stern, D., Eisenhardt, P. R. M., et al. 2009, *The Astrophysical Journal*, 694, 1309. <https://ui.adsabs.harvard.edu/abs/2009ApJ...694.1309G/abstract>
- Gardner, J. P., Mather, J. C., Abbott, R., et al. 2023, *Publications of the Astronomical Society of the Pacific*, 135, 068001, aDS Bibcode: 2023PASP..135f8001G. <https://ui.adsabs.harvard.edu/abs/2023PASP..135f8001G>
- Geha, M., Blanton, M. R., Yan, R., & Tinker, J. L. 2012, *The Astrophysical Journal*, 757, 85. <https://ui.adsabs.harvard.edu/abs/2012ApJ...757...85G/abstract>
- Genin, A., Shuntov, M., Brammer, G., et al. 2025, eprint arXiv:2505.21622, arXiv:2505.21622. <https://ui.adsabs.harvard.edu/abs/2025arXiv250521622G/abstract>
- George, K. 2017, *Astronomy and Astrophysics*, 598, A45. <https://ui.adsabs.harvard.edu/abs/2017A&A...598A..45G/abstract>
- . 2023, *Astronomy and Astrophysics*, 678, A10. <https://ui.adsabs.harvard.edu/abs/2023A&A...678A..10G/abstract>
- George, K., & Zingade, K. 2015, *Astronomy and Astrophysics*, 583, A103. <https://ui.adsabs.harvard.edu/abs/2015A&A...583A.103G/abstract>
- Gobat, R., Daddi, E., Onodera, M., et al. 2011, *Astronomy and Astrophysics*, 526, A133. <https://ui.adsabs.harvard.edu/abs/2011A&A...526A.133G/abstract>
- Gobat, R., Strazzullo, V., Daddi, E., et al. 2013, *The Astrophysical Journal*, 776, 9. <https://ui.adsabs.harvard.edu/abs/2013ApJ...776....9G/abstract>
- Gunn, J. E., & Gott, J. R. 1972, *The Astrophysical Journal*, 176, 1. <https://ui.adsabs.harvard.edu/abs/1972ApJ...176....1G/abstract>
- Guo, Y., Ferguson, H. C., Giavalisco, M., et al. 2013, *The Astrophysical Journal Supplement Series*, 207, 24. <https://ui.adsabs.harvard.edu/abs/2013ApJS..207...24G/abstract>
- Haggard, R., Gray, M. E., Pearce, F. R., et al. 2020, *Monthly Notices of the Royal Astronomical Society*, 492, 6074. <https://ui.adsabs.harvard.edu/abs/2020MNRAS.492.6074H/abstract>
- Hahn, O., Carollo, C. M., Porciani, C., & Dekel, A. 2007, *Monthly Notices of the Royal Astronomical Society*, 381, 41. <https://ui.adsabs.harvard.edu/abs/2007MNRAS.381..41H/abstract>
- Hainline, K. N., Reines, A. E., Greene, J. E., & Stern, D. 2016, *The Astrophysical Journal*, 832, 119. <https://ui.adsabs.harvard.edu/abs/2016ApJ...832..119H/abstract>
- Hainline, K. N., Johnson, B. D., Robertson, B., et al. 2024, *The Astrophysical Journal*, 964, 71, aDS Bibcode: 2024ApJ...964...71H. <https://ui.adsabs.harvard.edu/abs/2024ApJ...964...71H>
- Hamadouche, M. L., Carnall, A. C., McLure, R. J., et al. 2022, *Monthly Notices of the Royal Astronomical Society*, 512, 1262. <https://ui.adsabs.harvard.edu/abs/2022MNRAS.512.1262H/abstract>
- Hamadouche, M. L., McLure, R. J., Carnall, A. C., et al. 2025, *Monthly Notices of the Royal Astronomical Society*, 541, 463. <https://ui.adsabs.harvard.edu/abs/2025MNRAS.541..463H/abstract>
- Harrold, J. E., Almaini, O., Pearce, F. R., et al. 2026, *Monthly Notices of the Royal Astronomical Society*, 545, staf2191. <https://ui.adsabs.harvard.edu/abs/2026MNRAS.545f2191H/abstract>
- Hashiguchi, A., Toba, Y., Ota, N., et al. 2023, *Publications of the Astronomical Society of Japan*, 75, 1246. <https://ui.adsabs.harvard.edu/abs/2023PASJ...75.1246H/abstract>
- Helton, J. M., Sun, F., Woodrum, C., et al. 2024, *The Astrophysical Journal*, 974, 41. <https://ui.adsabs.harvard.edu/abs/2024ApJ...974...41H/abstract>
- Henriques, B. M. B., White, S. D. M., Thomas, P. A., et al. 2015, *Monthly Notices of the Royal Astronomical Society*, 451, 2663. <https://ui.adsabs.harvard.edu/abs/2015MNRAS.451.2663H/abstract>
- . 2017, *Monthly Notices of the Royal Astronomical Society*, 469, 2626. <https://ui.adsabs.harvard.edu/abs/2017MNRAS.469.2626H/abstract>
- Huchra, J. P., & Geller, M. J. 1982, *The Astrophysical Journal*, 257, 423. <https://ui.adsabs.harvard.edu/abs/1982ApJ...257..423H/abstract>
- Iani, E., Rinaldi, P., Caputi, K. I., et al. 2024, MIDIS: MIRI uncovers Virgil, an extended source at  $z \sim 6.6$  with the photometric properties of Little Red Dots, , publication Title: arXiv e-prints ADS Bibcode: 2024arXiv240618207I, doi:10.48550/arXiv.2406.18207. <https://ui.adsabs.harvard.edu/abs/2024arXiv240618207I>

- Ito, K., Valentino, F., Baker, W. M., et al. 2026, arXiv e-prints, arXiv:2601.01722. <https://ui.adsabs.harvard.edu/abs/2026arXiv260101722I/abstract>
- Jaffé, Y. L., Smith, R., Candlish, G. N., et al. 2015, *Monthly Notices of the Royal Astronomical Society*, 448, 1715. <https://ui.adsabs.harvard.edu/abs/2015MNRAS.448.1715J/abstract>
- Jakobsen, P., Ferruit, P., Alves de Oliveira, C., et al. 2022, *Astronomy and Astrophysics*, 661, A80, aDS Bibcode: 2022A&A...661A..80J. <https://ui.adsabs.harvard.edu/abs/2022A&A...661A..80J>
- Jee, M. J., Dawson, K. S., Hoekstra, H., et al. 2011, *The Astrophysical Journal*, 737, 59. <https://ui.adsabs.harvard.edu/abs/2011ApJ...737...59J/abstract>
- Ji, Z., Giavalisco, M., Williams, C. C., et al. 2018, *The Astrophysical Journal*, 862, 135. <https://ui.adsabs.harvard.edu/abs/2018ApJ...862..135J/abstract>
- Kauffmann, G., White, S. D. M., Heckman, T. M., et al. 2004, *Monthly Notices of the Royal Astronomical Society*, 353, 713. <https://ui.adsabs.harvard.edu/abs/2004MNRAS.353..713K/abstract>
- Kawinwanichakij, L., Papovich, C., Quadri, R. F., et al. 2017, *The Astrophysical Journal*, 847, 134. <https://ui.adsabs.harvard.edu/abs/2017ApJ...847..134K/abstract>
- Kennicutt, R. C., & Evans, N. J. 2012, *Annual Review of Astronomy and Astrophysics*, 50, 531, aDS Bibcode: 2012ARA&A..50..531K. <https://ui.adsabs.harvard.edu/abs/2012ARA&A..50..531K>
- Kim, K. J., Bayliss, M. B., Noble, A. G., et al. 2023, *The Astrophysical Journal*, 955, 32. <https://ui.adsabs.harvard.edu/abs/2023ApJ...955...32K/abstract>
- Kiyota, T., Ando, M., Tanaka, M., et al. 2025, *The Astrophysical Journal*, 980, 104. <https://ui.adsabs.harvard.edu/abs/2025ApJ...980..104K/abstract>
- Kollmeier, J. A., Rix, H.-W., Aerts, C., et al. 2025, arXiv e-prints, arXiv:2507.06989. <https://ui.adsabs.harvard.edu/abs/2025arXiv250706989K/abstract>
- Kravtsov, A. V., & Borgani, S. 2012, *Annual Review of Astronomy and Astrophysics*, 50, 353. <https://ui.adsabs.harvard.edu/abs/2012ARA&A..50..353K/abstract>
- Kroupa, P. 2001, *Monthly Notices of the Royal Astronomical Society*, 322, 231, aDS Bibcode: 2001MNRAS.322..231K. <https://ui.adsabs.harvard.edu/abs/2001MNRAS.322..231K>
- Kuchner, U., Ziegler, B., Verdugo, M., Bamford, S., & Häußler, B. 2017, *Astronomy and Astrophysics*, 604, A54. <https://ui.adsabs.harvard.edu/abs/2017A&A...604A..54K/abstract>
- Kuhn, V., Guo, Y., Martin, A., et al. 2024, *The Astrophysical Journal*, 968, L15. <https://ui.adsabs.harvard.edu/abs/2024ApJ...968L..15K/abstract>
- Lee-Brown, D. B., Rudnick, G. H., Momcheva, I. G., et al. 2017, *The Astrophysical Journal*, 844, 43. <https://ui.adsabs.harvard.edu/abs/2017ApJ...844...43L/abstract>
- Leja, J., Carnall, A. C., Johnson, B. D., Conroy, C., & Speagle, J. S. 2019, *The Astrophysical Journal*, 876, 3, aDS Bibcode: 2019ApJ...876....3L. <https://ui.adsabs.harvard.edu/abs/2019ApJ...876....3L>
- Leja, J., Speagle, J. S., Ting, Y.-S., et al. 2022, *The Astrophysical Journal*, 936, 165. <https://ui.adsabs.harvard.edu/abs/2022ApJ...936..165L/abstract>
- Li, Q., Conselice, C. J., Sarron, F., et al. 2025, *Monthly Notices of the Royal Astronomical Society*, 539, 1796. <https://ui.adsabs.harvard.edu/abs/2025MNRAS.539.1796L/abstract>
- Lim, S., Scott, D., Babul, A., et al. 2021, *Monthly Notices of the Royal Astronomical Society*, 501, 1803. <https://ui.adsabs.harvard.edu/abs/2021MNRAS.501.1803L/abstract>
- Lim, S., Tacchella, S., Schaye, J., et al. 2024, *Monthly Notices of the Royal Astronomical Society*, 532, 4551. <https://ui.adsabs.harvard.edu/abs/2024MNRAS.532.4551L/abstract>
- Liu, S., Gu, Y., Yuan, Q., et al. 2021, *The Astrophysical Journal*, 923, 46. <https://ui.adsabs.harvard.edu/abs/2021ApJ...923...46L/abstract>
- Looser, T. J., D'Eugenio, F., Maiolino, R., et al. 2024, *Nature*, 629, 53, aDS Bibcode: 2024Natur.629...53L. <https://ui.adsabs.harvard.edu/abs/2024Natur.629...53L>
- Lu, Y., Yang, X., Shi, F., et al. 2016, *The Astrophysical Journal*, 832, 39. <https://ui.adsabs.harvard.edu/abs/2016ApJ...832...39L/abstract>
- Luo, B., Brandt, W. N., Xue, Y. Q., et al. 2017, *The Astrophysical Journal Supplement Series*, 228, 2, aDS Bibcode: 2017ApJS..228....2L. <https://ui.adsabs.harvard.edu/abs/2017ApJS..228....2L>
- Lyu, J., Alberts, S., Rieke, G. H., & Rujopakarn, W. 2022, *The Astrophysical Journal*, 941, 191, aDS Bibcode: 2022ApJ...941..191L. <https://ui.adsabs.harvard.edu/abs/2022ApJ...941..191L>
- Lyu, J., Alberts, S., Rieke, G. H., et al. 2024, *The Astrophysical Journal*, 966, 229, aDS Bibcode: 2024ApJ...966..229L. <https://ui.adsabs.harvard.edu/abs/2024ApJ...966..229L>
- Ma, H.-X., Takeuchi, T. T., Cooray, S., & Zhu, Y. 2025, *Monthly Notices of the Royal Astronomical Society*, 537, 1504. <https://ui.adsabs.harvard.edu/abs/2025MNRAS.537.1504M/abstract>

- Mantz, A. B., Allen, S. W., Morris, R. G., et al. 2020, *Monthly Notices of the Royal Astronomical Society*, 496, 1554. <https://ui.adsabs.harvard.edu/abs/2020MNRAS.496.1554M/abstract>
- Martini, P., Miller, E. D., Brodwin, M., et al. 2013, *The Astrophysical Journal*, 768, 1. <https://ui.adsabs.harvard.edu/abs/2013ApJ...768....1M/abstract>
- Martorano, M., van der Wel, A., Baes, M., et al. 2024, *The Astrophysical Journal*, 972, 134. <https://ui.adsabs.harvard.edu/abs/2024ApJ...972..134M/abstract>
- McGee, S. L., Balogh, M. L., Bower, R. G., Font, A. S., & McCarthy, I. G. 2009, *Monthly Notices of the Royal Astronomical Society*, 400, 937. <https://ui.adsabs.harvard.edu/abs/2009MNRAS.400..937M/abstract>
- McNab, K., Balogh, M. L., van der Burg, R. F. J., et al. 2021, *Monthly Notices of the Royal Astronomical Society*, 508, 157. <https://ui.adsabs.harvard.edu/abs/2021MNRAS.508..157M/abstract>
- McQuinn, K. B. W., van Zee, L., & Skillman, E. D. 2019, *The Astrophysical Journal*, 886, 74. <https://ui.adsabs.harvard.edu/abs/2019ApJ...886...74M/abstract>
- Mei, S., Holden, B. P., Blakeslee, J. P., et al. 2009, *The Astrophysical Journal*, 690, 42. <https://ui.adsabs.harvard.edu/abs/2009ApJ...690...42M/abstract>
- Mei, S., Scarlata, C., Pentericci, L., et al. 2015, *The Astrophysical Journal*, 804, 117, aDS Bibcode: 2015ApJ...804..117M. <https://ui.adsabs.harvard.edu/abs/2015ApJ...804..117M>
- Mei, S., Hatch, N. A., Amodeo, S., et al. 2023, *Astronomy and Astrophysics*, 670, A58. <https://ui.adsabs.harvard.edu/abs/2023A&A...670A..58M/abstract>
- Meidt, S. E., Schinnerer, E., van de Ven, G., et al. 2014, *The Astrophysical Journal*, 788, 144. <https://ui.adsabs.harvard.edu/abs/2014ApJ...788..144M/abstract>
- Menanteau, F., Hughes, J. P., Sifón, C., et al. 2012, *The Astrophysical Journal*, 748, 7. <https://ui.adsabs.harvard.edu/abs/2012ApJ...748....7M/abstract>
- Miller, T. B., Chapman, S. C., Aravena, M., et al. 2018, *Nature*, 556, 469. <https://ui.adsabs.harvard.edu/abs/2018Natur.556..469M/abstract>
- Moore, B., Lake, G., & Katz, N. 1998, *The Astrophysical Journal*, 495, 139. <https://ui.adsabs.harvard.edu/abs/1998ApJ...495..139M/abstract>
- Muldrew, S. I., Hatch, N. A., & Cooke, E. A. 2015, *Monthly Notices of the Royal Astronomical Society*, 452, 2528. <https://ui.adsabs.harvard.edu/abs/2015MNRAS.452.2528M/abstract>
- Munari, E., Biviano, A., Borgani, S., Murante, G., & Fabjan, D. 2013, *Monthly Notices of the Royal Astronomical Society*, 430, 2638. <https://ui.adsabs.harvard.edu/abs/2013MNRAS.430.2638M/abstract>
- Muzzin, A., Wilson, G., Demarco, R., et al. 2013, *The Astrophysical Journal*, 767, 39. <https://ui.adsabs.harvard.edu/abs/2013ApJ...767...39M/abstract>
- Muzzin, A., Wilson, G., Yee, H. K. C., et al. 2012, *The Astrophysical Journal*, 746, 188. <https://ui.adsabs.harvard.edu/abs/2012ApJ...746..188M/abstract>
- Mérida, R. M., Sawicki, M., Iyer, K. G., et al. 2025, arXiv e-prints, arXiv:2509.22871. <https://ui.adsabs.harvard.edu/abs/2025arXiv250922871M/abstract>
- Navarro-Carrera, R., Rinaldi, P., Caputi, K. I., et al. 2024a, *Burstiness in low stellar-mass Ha emitters at  $z \sim 2$  and  $z \sim 4-6$  from JWST medium band photometry in GOODS-S*, , publication Title: arXiv e-prints ADS Bibcode: 2024arXiv241023249N, doi:10.48550/arXiv.2410.23249. <https://ui.adsabs.harvard.edu/abs/2024arXiv241023249N>
- . 2024b, *The Astrophysical Journal*, 961, 207, aDS Bibcode: 2024ApJ...961..207N. <https://ui.adsabs.harvard.edu/abs/2024ApJ...961..207N>
- Nelson, D., Pillepich, A., Ayromlou, M., et al. 2024, *Astronomy and Astrophysics*, 686, A157. <https://ui.adsabs.harvard.edu/abs/2024A&A...686A.157N/abstract>
- Nelson, D., Springel, V., Pillepich, A., et al. 2019, *Computational Astrophysics and Cosmology*, 6, 2. <https://ui.adsabs.harvard.edu/abs/2019ComAC...6....2N/abstract>
- Newman, A. B., Ellis, R. S., Andreon, S., et al. 2014, *The Astrophysical Journal*, 788, 51. <https://ui.adsabs.harvard.edu/abs/2014ApJ...788...51N/abstract>
- Nielsen, E. W., Steinhardt, C. L., Harper, M., McPartland, C., & Sedgewick, A. 2025, *Astronomy and Astrophysics*, 700, A116. <https://ui.adsabs.harvard.edu/abs/2025A&A...700A.116N/abstract>
- Noble, A. G., Webb, T. M. A., Muzzin, A., et al. 2013, *The Astrophysical Journal*, 768, 118. <https://ui.adsabs.harvard.edu/abs/2013ApJ...768..118N/abstract>
- Noble, A. G., Webb, T. M. A., Yee, H. K. C., et al. 2016, *The Astrophysical Journal*, 816, 48. <https://ui.adsabs.harvard.edu/abs/2016ApJ...816...48N/abstract>
- Noiro, G., Stern, D., Mei, S., et al. 2018, *The Astrophysical Journal*, 859, 38. <https://ui.adsabs.harvard.edu/abs/2018ApJ...859...38N/abstract>
- Noiro, G., Desprez, G., Asada, Y., et al. 2023, *Monthly Notices of the Royal Astronomical Society*, 525, 1867. <https://ui.adsabs.harvard.edu/abs/2023MNRAS.525.1867N/abstract>

- Nolan, L. A., Raychaudhury, S., & Kabán, A. 2007, *Monthly Notices of the Royal Astronomical Society*, 375, 381. <https://ui.adsabs.harvard.edu/abs/2007MNRAS.375..381N/abstract>
- Noordeh, E., Canning, R. E. A., Willis, J. P., et al. 2021, *Monthly Notices of the Royal Astronomical Society*, 507, 5272. <https://ui.adsabs.harvard.edu/abs/2021MNRAS.507.5272N/abstract>
- Oesch, P. A., Brammer, G., Naidu, R. P., et al. 2023, *Monthly Notices of the Royal Astronomical Society*, 525, 2864, aDS Bibcode: 2023MNRAS.525.2864O. <https://ui.adsabs.harvard.edu/abs/2023MNRAS.525.2864O>
- Oke, J. B., & Gunn, J. E. 1983, *The Astrophysical Journal*, 266, 713, aDS Bibcode: 1983ApJ...266..713O. <https://ui.adsabs.harvard.edu/abs/1983ApJ...266..713O>
- Overzier, R. A. 2016, *Astronomy and Astrophysics Review*, 24, 14. <https://ui.adsabs.harvard.edu/abs/2016A&ARv..24...14O/abstract>
- Pacifici, C., Kassin, S. A., Weiner, B. J., et al. 2016, *The Astrophysical Journal*, 832, 79. <https://ui.adsabs.harvard.edu/abs/2016ApJ...832...79P/abstract>
- Pan, R., Suess, K. A., Marchesini, D., et al. 2025, *The Astrophysical Journal*, 990, L24. <https://ui.adsabs.harvard.edu/abs/2025ApJ...990L..24P/abstract>
- Papovich, C., Momcheva, I., Willmer, C. N. A., et al. 2010, *The Astrophysical Journal*, 716, 1503. <https://ui.adsabs.harvard.edu/abs/2010ApJ...716.1503P/abstract>
- Papovich, C., Kawinwanichakij, L., Quadri, R. F., et al. 2018, *The Astrophysical Journal*, 854, 30. <https://ui.adsabs.harvard.edu/abs/2018ApJ...854...30P/abstract>
- Pasha, I., & Miller, T. B. 2023, *The Journal of Open Source Software*, 8, 5703. <https://ui.adsabs.harvard.edu/abs/2023JOSS...8.5703P/abstract>
- Peng, Y.-j., Lilly, S. J., Renzini, A., & Carollo, M. 2012, *The Astrophysical Journal*, 757, 4. <https://ui.adsabs.harvard.edu/abs/2012ApJ...757....4P/abstract>
- Peng, Y.-j., Lilly, S. J., Kovač, K., et al. 2010, *The Astrophysical Journal*, 721, 193. <https://ui.adsabs.harvard.edu/abs/2010ApJ...721..193P/abstract>
- Pintos-Castro, I., Yee, H. K. C., Muzzin, A., Old, L., & Wilson, G. 2019, *The Astrophysical Journal*, 876, 40. <https://ui.adsabs.harvard.edu/abs/2019ApJ...876...40P/abstract>
- Poggianti, B. M., & Barbaro, G. 1997, *Astronomy and Astrophysics*, 325, 1025. <https://ui.adsabs.harvard.edu/abs/1997A&A...325.1025P/abstract>
- Polletta, M., Soucail, G., Dole, H., et al. 2021, *Astronomy and Astrophysics*, 654, A121. <https://ui.adsabs.harvard.edu/abs/2021A&A...654A.121P/abstract>
- Popesso, P., Biviano, A., Rodighiero, G., et al. 2012, *Astronomy and Astrophysics*, 537, A58. <https://ui.adsabs.harvard.edu/abs/2012A&A...537A..58P/abstract>
- Press, W. H., & Schechter, P. 1974, *The Astrophysical Journal*, 187, 425. <https://ui.adsabs.harvard.edu/abs/1974ApJ...187..425P/abstract>
- Ramella, M., Boschin, W., Fadda, D., & Nonino, M. 2001, *Astronomy and Astrophysics*, 368, 776. <https://ui.adsabs.harvard.edu/abs/2001A&A...368..776R/abstract>
- Rettura, A., Mei, S., Stanford, S. A., et al. 2011, *The Astrophysical Journal*, 732, 94. <https://ui.adsabs.harvard.edu/abs/2011ApJ...732...94R/abstract>
- Rhee, J., Smith, R., Choi, H., et al. 2017, *The Astrophysical Journal*, 843, 128. <https://ui.adsabs.harvard.edu/abs/2017ApJ...843..128R/abstract>
- Rieke, G. H., Alberts, S., Shivaeei, I., et al. 2024, *The Astrophysical Journal*, 975, 83, aDS Bibcode: 2024ApJ...975...83R. <https://ui.adsabs.harvard.edu/abs/2024ApJ...975...83R>
- Rieke, M. J., Kelly, D. M., Misselt, K., et al. 2023, *Publications of the Astronomical Society of the Pacific*, 135, 028001, aDS Bibcode: 2023PASP..135b8001R. <https://ui.adsabs.harvard.edu/abs/2023PASP..135b8001R>
- Rinaldi, P., Caputi, K. I., van Mierlo, S. E., et al. 2022, *The Astrophysical Journal*, 930, 128. <https://ui.adsabs.harvard.edu/abs/2022ApJ...930..128R/abstract>
- Rinaldi, P., Caputi, K. I., Costantin, L., et al. 2023, *The Astrophysical Journal*, 952, 143, aDS Bibcode: 2023ApJ...952..143R. <https://ui.adsabs.harvard.edu/abs/2023ApJ...952..143R>
- Rinaldi, P., Navarro-Carrera, R., Caputi, K. I., et al. 2024, *The emergence of the Star Formation Main Sequence with redshift unfolded by JWST*, , , publication Title: arXiv e-prints ADS Bibcode: 2024arXiv240613554R, doi:10.48550/arXiv.2406.13554. <https://ui.adsabs.harvard.edu/abs/2024arXiv240613554R>
- Rinaldi, P., Pérez-González, P. G., Rieke, G. H., et al. 2025, arXiv e-prints, arXiv:2504.01852. <https://ui.adsabs.harvard.edu/abs/2025arXiv250401852R/abstract>
- Roberts, I. D., Parker, L. C., Brown, T., et al. 2019, *The Astrophysical Journal*, 873, 42. <https://ui.adsabs.harvard.edu/abs/2019ApJ...873...42R/abstract>
- Roberts, I. D., van Weeren, R. J., Timmerman, R., et al. 2022, *Astronomy and Astrophysics*, 658, A44. <https://ui.adsabs.harvard.edu/abs/2022A&A...658A..44R/abstract>
- Rykoff, E. S., Evrard, A. E., McKay, T. A., et al. 2008, *Monthly Notices of the Royal Astronomical Society*, 387, L28. <https://ui.adsabs.harvard.edu/abs/2008MNRAS.387L..28R/abstract>

- Sarazin, C. L. 1986, *Reviews of Modern Physics*, 58, 1. <https://ui.adsabs.harvard.edu/abs/1986RvMP...58....1S/abstract>
- Schaye, J., Kugel, R., Schaller, M., et al. 2023, *Monthly Notices of the Royal Astronomical Society*, 526, 4978. <https://ui.adsabs.harvard.edu/abs/2023MNRAS.526.4978S/abstract>
- Shah, E. A., Lemaux, B. C., Forrest, B., et al. 2025, *Astronomy and Astrophysics*, 704, A101. <https://ui.adsabs.harvard.edu/abs/2025A&A...704A.101S/abstract>
- Shen, L., Papovich, C., Matharu, J., et al. 2024, *The Astrophysical Journal*, 963, L49. <https://ui.adsabs.harvard.edu/abs/2024ApJ...963L..49S/abstract>
- . 2025, *The Astrophysical Journal*, 980, L45. <https://ui.adsabs.harvard.edu/abs/2025ApJ...980L..45S/abstract>
- Shuntov, M., McCracken, H. J., Gavazzi, R., et al. 2022, *Astronomy and Astrophysics*, 664, A61. <https://ui.adsabs.harvard.edu/abs/2022A&A...664A..61S/abstract>
- Simmonds, C., Tacchella, S., Curtis-Lake, W. M. E., et al. 2025, *Monthly Notices of the Royal Astronomical Society*, doi:10.1093/mnras/staf1950. <https://ui.adsabs.harvard.edu/abs/2025MNRAS.tmp.1832S/abstract>
- Smail, I. 2024, *Monthly Notices of the Royal Astronomical Society*, 529, 2290. <https://ui.adsabs.harvard.edu/abs/2024MNRAS.529.2290S/abstract>
- Speagle, J. S., Steinhardt, C. L., Capak, P. L., & Silverman, J. D. 2014, *The Astrophysical Journal Supplement Series*, 214, 15. <https://ui.adsabs.harvard.edu/abs/2014ApJS..214..15S/abstract>
- Stanford, S. A., Brodwin, M., Gonzalez, A. H., et al. 2012, *The Astrophysical Journal*, 753, 164. <https://ui.adsabs.harvard.edu/abs/2012ApJ...753..164S/abstract>
- Strazzullo, V., Pannella, M., Mohr, J. J., et al. 2019, *Astronomy and Astrophysics*, 622, A117. <https://ui.adsabs.harvard.edu/abs/2019A&A...622A.117S/abstract>
- Sun, H., Wang, T., Xu, K., et al. 2024, *The Astrophysical Journal*, 967, L34. <https://ui.adsabs.harvard.edu/abs/2024ApJ...967L..34S/abstract>
- Tacchella, S., Dekel, A., Carollo, C. M., et al. 2016, *Monthly Notices of the Royal Astronomical Society*, 457, 2790. <https://ui.adsabs.harvard.edu/abs/2016MNRAS.457.2790T/abstract>
- Thomas, D., Maraston, C., Bender, R., & Mendes de Oliveira, C. 2005, *The Astrophysical Journal*, 621, 673. <https://ui.adsabs.harvard.edu/abs/2005ApJ...621..673T/abstract>
- Thomas, D., Maraston, C., Schawinski, K., Sarzi, M., & Silk, J. 2010, *Monthly Notices of the Royal Astronomical Society*, 404, 1775. <https://ui.adsabs.harvard.edu/abs/2010MNRAS.404.1775T/abstract>
- Tomczak, A. R., Lemaux, B. C., Lubin, L. M., et al. 2017, *Monthly Notices of the Royal Astronomical Society*, 472, 3512. <https://ui.adsabs.harvard.edu/abs/2017MNRAS.472.3512T/abstract>
- Umehata, H., Tamura, Y., Kohno, K., et al. 2015, *The Astrophysical Journal*, 815, L8. <https://ui.adsabs.harvard.edu/abs/2015ApJ...815L..8U/abstract>
- van der Burg, R. F. J., Rudnick, G., Balogh, M. L., et al. 2020, *Astronomy and Astrophysics*, 638, A112. <https://ui.adsabs.harvard.edu/abs/2020A&A...638A.112V/abstract>
- Wagner, C. R., Brodwin, M., Snyder, G. F., et al. 2015, *The Astrophysical Journal*, 800, 107. <https://ui.adsabs.harvard.edu/abs/2015ApJ...800..107W/abstract>
- Walter, F., Decarli, R., Aravena, M., et al. 2016, *The Astrophysical Journal*, 833, 67. <https://ui.adsabs.harvard.edu/abs/2016ApJ...833..67W/abstract>
- Wang, T., Elbaz, D., Daddi, E., et al. 2016, *The Astrophysical Journal*, 828, 56. <https://ui.adsabs.harvard.edu/abs/2016ApJ...828..56W/abstract>
- . 2018, *The Astrophysical Journal*, 867, L29. <https://ui.adsabs.harvard.edu/abs/2018ApJ...867L..29W/abstract>
- Watson, C. B., Blanton, E. L., Golden-Marx, E., et al. 2025a, *The Astrophysical Journal*, 984, 57. <https://ui.adsabs.harvard.edu/abs/2025ApJ...984..57W/abstract>
- Watson, P. J., Vulcani, B., Treu, T., et al. 2025b, *arXiv e-prints*, arXiv:2504.00823. <https://ui.adsabs.harvard.edu/abs/2025arXiv250400823W/abstract>
- Webb, K., Balogh, M. L., Leja, J., et al. 2020, *Monthly Notices of the Royal Astronomical Society*, 498, 5317. <https://ui.adsabs.harvard.edu/abs/2020MNRAS.498.5317W/abstract>
- Webb, T. M. A., O'Donnell, D., Yee, H. K. C., et al. 2013, *The Astronomical Journal*, 146, 84. <https://ui.adsabs.harvard.edu/abs/2013AJ...146..84W/abstract>
- Werner, S. V., Hatch, N. A., Muzzin, A., et al. 2022, *Monthly Notices of the Royal Astronomical Society*, 510, 674. <https://ui.adsabs.harvard.edu/abs/2022MNRAS.510..674W/abstract>
- Whitaker, K. E., van Dokkum, P. G., Brammer, G., & Franx, M. 2012, *The Astrophysical Journal*, 754, L29. <https://ui.adsabs.harvard.edu/abs/2012ApJ...754L..29W/abstract>
- Whitaker, K. E., Labbé, I., van Dokkum, P. G., et al. 2011, *The Astrophysical Journal*, 735, 86. <https://ui.adsabs.harvard.edu/abs/2011ApJ...735..86W/abstract>
- Whitaker, K. E., Ashas, M., Illingworth, G., et al. 2019, *The Astrophysical Journal Supplement Series*, 244, 16, aDS Bibcode: 2019ApJS..244..16W. <https://ui.adsabs.harvard.edu/abs/2019ApJS..244..16W>

- White, S. D. M., & Rees, M. J. 1978, *Monthly Notices of the Royal Astronomical Society*, 183, 341. <https://ui.adsabs.harvard.edu/abs/1978MNRAS.183..341W/abstract>
- Wilkins, S. M., Lovell, C. C., Irodotou, D., et al. 2024, *Monthly Notices of the Royal Astronomical Society*, 527, 7965. <https://ui.adsabs.harvard.edu/abs/2024MNRAS.527.7965W/abstract>
- Williams, C. C., Alberts, S., Spilker, J. S., et al. 2022, *The Astrophysical Journal*, 929, 35. <https://ui.adsabs.harvard.edu/abs/2022ApJ...929...35W/abstract>
- Williams, C. C., Tacchella, S., Maseda, M. V., et al. 2023, *The Astrophysical Journal Supplement Series*, 268, 64, aDS Bibcode: 2023ApJS..268...64W. <https://ui.adsabs.harvard.edu/abs/2023ApJS..268...64W>
- Williams, R. J., Quadri, R. F., Franx, M., van Dokkum, P., & Labbé, I. 2009, *The Astrophysical Journal*, 691, 1879. <https://ui.adsabs.harvard.edu/abs/2009ApJ...691.1879W/abstract>
- Williamson, R., Benson, B. A., High, F. W., et al. 2011, *The Astrophysical Journal*, 738, 139. <https://ui.adsabs.harvard.edu/abs/2011ApJ...738..139W/abstract>
- Willott, C. J., Doyon, R., Albert, L., et al. 2022, *Publications of the Astronomical Society of the Pacific*, 134, 025002. <https://ui.adsabs.harvard.edu/abs/2022PASP..134b5002W/abstract>
- Witten, C., Oesch, P. A., Bennett, J. S., et al. 2025, arXiv e-prints, arXiv:2511.05647. <https://ui.adsabs.harvard.edu/abs/2025arXiv251105647W/abstract>
- Worthey, G., Faber, S. M., Gonzalez, J. J., & Burstein, D. 1994, *The Astrophysical Journal Supplement Series*, 94, 687. <https://ui.adsabs.harvard.edu/abs/1994ApJS...94..687W/abstract>
- Wright, G. S., Rieke, G. H., Glasse, A., et al. 2023, *Publications of the Astronomical Society of the Pacific*, 135, 048003, aDS Bibcode: 2023PASP..135d8003W. <https://ui.adsabs.harvard.edu/abs/2023PASP..135d8003W>
- Wu, Z., Eisenstein, D. J., Johnson, B. D., et al. 2026, arXiv e-prints, arXiv:2601.15960. <https://ui.adsabs.harvard.edu/abs/2026arXiv260115960W/abstract>
- Wylezalek, D., Galametz, A., Stern, D., et al. 2013, *The Astrophysical Journal*, 769, 79. <https://ui.adsabs.harvard.edu/abs/2013ApJ...769...79W/abstract>
- Wylezalek, D., Vernet, J., De Breuck, C., et al. 2014, *The Astrophysical Journal*, 786, 17. <https://ui.adsabs.harvard.edu/abs/2014ApJ...786...17W/abstract>
- Xue, Y. Q., Luo, B., Brandt, W. N., et al. 2011, *The Astrophysical Journal Supplement Series*, 195, 10. <https://ui.adsabs.harvard.edu/abs/2011ApJS..195...10X/abstract>
- Yahil, A., & Vidal, N. V. 1977, *The Astrophysical Journal*, 214, 347. <https://ui.adsabs.harvard.edu/abs/1977ApJ...214..347Y/abstract>
- Zhang, Z., Wang, H., Luo, W., et al. 2024, *The Astrophysical Journal*, 960, 71. <https://ui.adsabs.harvard.edu/abs/2024ApJ...960...71Z/abstract>
- Zheng, Y.-L., Yang, X., He, M., et al. 2023, *Monthly Notices of the Royal Astronomical Society*, 523, 4909. <https://ui.adsabs.harvard.edu/abs/2023MNRAS.523.4909Z/abstract>
- Zhu, Y., Bonaventura, N., Sun, Y., et al. 2025, arXiv e-prints, arXiv:2508.12599. <https://ui.adsabs.harvard.edu/abs/2025arXiv250812599Z/abstract>
- Zhu, Y., Rieke, M. J., Ji, Z., et al. 2026, arXiv e-prints, arXiv:2601.15965. <https://ui.adsabs.harvard.edu/abs/2026arXiv260115965Z/abstract>